12-2008

Application of Structural Control for Civil Engineering Structures

Abdollah Shafieezadeh
Utah State University

APPLICATION OF STRUCTURAL CONTROL FOR CIVIL ENGINEERING STRUCTURES

by

Abdollah Shafieezadeh

A thesis submitted in partial fulfillment
of the requirements for the degree

of

MASTER OF SCIENCE

in

Civil Engineering

Approved:

Keri Ryan Major Professor	YangQuan Chen Committee Member
Marvin Halling Committee Member	Byron R. Burnham Dean of Graduate Studies

UTAH STATE UNIVERSITY
Logan, Utah

2008

ABSTRACT

Application of Structural Control for Civil Engineering Structures

by

Abdollah Shafieezadeh, Master of Science

Utah State University, 2008

Major Professor: Dr. Keri L. Ryan
Department: Civil and Environmental Engineering

This study presents the application of control methods in seismic mitigation of structural responses. The study consists of two parts. In the first section, fractional order filters are utilized to enhance the performance of the conventional LQR method for optimal robust control of a simple civil structure. The introduced filters modify the state variables fed back to the constant gain controller. Four combinations of fractional order filter and LQR are considered and optimized based on a new performance criterion defined in the paper. Introducing fractional order filters is shown to improve the results considerably for both the artificially generated ground motions and previously recorded earthquake data. In the second part, frequency dependent filters are introduced to improve the effectiveness of active control systems designed to mitigate the seismic response of large scale civil structures. These filters are introduced as band pass pre-filters to the optimally designed H2/LQG controller to reduce the maximum singular value response of input-output transfer matrices over a defined frequency range. Furthermore, a structured uncertainty model is proposed to evaluate robustness of

stability and performance considering nonlinear force-deformation behavior of structures. The proposed perturbation model characterizes variations in the stiffness matrix more accurately, thereby reducing overconservatism in the estimated destabilizing perturbations. The aforementioned techniques are applied to the nonlinear SAC three story steel building. Numerical results indicate that introducing filters can enhance the performance of the system in almost all response measures, while preserving robustness of stability and performance.

(70 pages)

ACKNOWLEDGMENTS

I wish to express my gratitude to my supervisor, Dr. Keri Ryan, who was abundantly helpful and offered invaluable assistance, support, and guidance. I am very appreciative of her unwavering support and the amount of freedom she granted me for pursuing my own ideas. Also, I would like to thank deeply Prof. YangQuan Chen for his great advice and very insightful ideas during the course of this study. I hope I will be able to continue collaboration with both of them for many years to come. Special thanks also to a member of the supervisory committee, Prof. Marvin Halling, for his assistance throughout the entire process.

Also, I give special thanks to my friends, Leila Tahvilian, Prayag Sayani, Leila Ahmadi, and Saleh Taghvaeian, for their help and for the great moments we had.

This research was made possible by a graduate research fellowship funded by the Utah Transportation Center, and I am extremely grateful and honored to have received this funding.

Lastly, and most importantly, I wish to thank my parents for their unconditional love and support throughout the years. To them I dedicate this thesis.

Abdollah Shafieezadeh

CONTENTS

LIST OF TABLES

LIST OF FIGURES

CHAPTER I

INTRODUCTION

Mitigation of structural responses against earthquakes and strong winds has always been a strong challenge for civil engineers. Besides life safety, enhanced performance objectives for the seismic response of civil structures in large earthquakes are increasingly targeted to avoid large economic losses associated with damage in structural and nonstructural components. Substantially improved performance can be achieved through the application of structural control methods, and the last two decades have led to major accomplishments in the development of control devices and algorithms to enhance the performance of structures.

Optimal control theories are amongst the most popular candidates in control of civil structures such that they are typically the baseline controllers against which new approaches are judged. When the structure is fully observed, linear quadratic regulators (LQR) are very powerful in disturbance rejection and have guaranteed robust stability properties.

Fractional order control (FOC) referred to a class of controllers that utilize fractional order operators as a part of their structure became popular in the control community in the last few decades. The idea of extending the integer order of differential operators (derivative and integral) to arbitrary real numbers is not new and has come a long way since Leibniz pointed out the idea in a letter to L'Hospital in 1695. However, the unfamiliar idea of taking fractional operator and lack of powerful computational resources prevented the wide use of fractional operators in engineering fields for a long time. Recently, fractional order calculus has found many applications in different fields

of science such as material modeling, theory of fractals, theory of control of dynamical systems, biological systems, signal processing, and etc. The pioneering works in FOC has been conducted by Manabe where he studied the frequency and the transient response of the non-integer integral and its application to control systems. Oustaloup proposed the CRONE (Commande Robuste d'Ordre Non Entier which means fractional order robust control) control system which is a frequency domain technique for the robust control of perturbed systems using the unity feedback configuration. The other major type of FOC is the $PI^{\lambda}D^{\mu}$ controller introduced by Podlubny; a generalization to the well established Proportional Integral Derivative (PID) controller in which the order of integral and derivative are arbitrary real numbers. The satisfactory performance of FOC in disturbance rejection and reference command tracking has been demonstrated through numerous investigations.

Since the input ground acceleration disturbances to the system are stochastic in nature, representing their power spectrum characteristics by static filters such as the Kanai-Tajimi filter cannot accurately capture the overall properties of the earthquake. A limited number of studies have introduced frequency domain techniques to enhance LQR/LQG controller performance. The application of frequency dependent weighting functions were studied to model the input excitation and to weigh regulated outputs in place of constant weighting matrices in LQG control method. Further improvements in response may be possible by using filters to adjust the frequency content of the input disturbance used to design the controller.

Unlike the LQR method, robustness of the LQG approach to uncertainties is not guaranteed and the control design should be checked for robustness for each specific

application. Uncertainties in modeling large scale structures result from imprecise information on system properties (e.g. mass, damping, and stiffness matrices) and input disturbances; and are compounded by the complex behavior of structures that respond in their nonlinear range. Perturbations techniques have been applied to check robustness of stability and performance, where uncertainty in system properties were represented by unstructured perturbation matrices or block diagonal perturbation matrices for mass, damping, and stiffness. In the block diagonal approach, each diagonal matrix is still an unstructured perturbation matrix. However, even more accurate results are achievable if structured uncertainty models are utilized for each of the perturbation matrices in the global block diagonal uncertainty model.

The application of FOC in the control of seismically excited civil structures has been introduced in this study where four variants of FOC were considered. The first three variants implemented FOC as a filter on the input to a coupled static gain, while the last controller applied FOC in conjunction with an optimal linear quadratic regulator (LQR). Simulation results for artificially generated and real recorded input ground accelerations on a linear 2-story shear building model with active controllers showed a considerable enhancement is achievable in different structural responses through the application of FOC.

Also investigated in this study is the performance improvement of optimally designed H_2/LQG controllers using band pass pre-filters, which provide the flexibility to shape the frequency response of input-output transfer matrices, thereby reducing their maximum singular value response over the frequencies of concern. Finally, a general approach using structured perturbation theory is presented which can verify robustness of

stability and performance of nonlinear structures. The structured perturbation model quantifies the stiffness variations induced by nonlinear force-deformation behavior of structural elements, and applies these variations as bounded structured uncertainties to the model stiffness matrix.

CHAPTER II

FRACTIONAL ORDER FILTER ENHANCED LQR FOR SEISMIC PROTECTION OF CIVIL STRUCTURES[1]

Abstract

This study presents fractional order filters to enhance the performance of the conventional LQR method for optimal robust control of a simple civil structure. The introduced filters modify the state variables fed back to the constant gain controller. Four combinations of fractional order filter and LQR are considered and optimized based on a new performance criterion defined in the paper. Introducing fractional order filters is shown to improve the results considerably for both the artificially generated ground motions and previously recorded earthquake data.

1 Introduction

Today, mitigating structural responses against natural hazards like earthquakes and strong winds has become one of the most challenging topics in structural engineering. Much research has been done on control devices to be implemented as structural elements and control algorithms applied to those devices to enhance the performance of the structure. Because of their simplicity and ease of use, of all the algorithms proposed for civil engineering structures, the linear quadratic regulator (LQR) and linear quadratic Gaussian (LQG) algorithms have become very popular. Indeed, they are usually used as a baseline for evaluation of other control schemes.

An overview of the applications of the LQR method in seismic excited structures has

[1] Coauthored by Abdollah Shafieezadeh, Keri Ryan, and YangQuan Chen

been given by Soong [1]. Yang et al. [2] proposed a scheme to include the effect of acceleration response in the control gain. This is achieved by adding a weighted acceleration component to the performance index and finding new gains in terms of state space variables. The effectiveness of an Instantaneous Optimal Controller applied to a 10-story steel building frame was investigated by Chang and Henry [3]. Ankireddi and Yang [4] implemented LQG controllers to control wind excited tall buildings. Controller parameters were obtained through optimization of a multi objective performance criterion in which the root mean square (RMS) response of the subjected structure and the control force were constrained to be less than some prescribed values due to practical issues. Guoping and Jinzhi [5] proposed the use of an optimal control method for seismic excited linear structures considering time delays by transforming the equations into discrete time form. The optimal controller gain was obtained directly from the time delay differential equation (DDE), and can therefore be available for the case of a large time delay. The H2/LQG method was implemented in a control scheme by Ramallo et al. [6] to evaluate semi-active control of a base-isolated building relative to passive isolation. To enforce the dissipation requirement for the semi-active device, a clipping secondary controller was used to filter the output of the H2/LQG controller. Simulation results for seismic-excited structures showed that smart dampers controlled by the H2/LQG algorithm can provide superior protection from a wide range of ground motions compared to the passive designs [6]. Adeli and Kim [7] presented a hybrid feedback-least mean square algorithm for control of structures through integration of the LQR or LQG algorithm and the filtered-x LMS method. Wang8 introduced an LQG-α controller, which considers robustness and extends the LQG control design method with a relative

stability and an adjustable gain parameter. The simulations of the controller on both wind and earthquake-excited buildings for some perturbations of the stiffness parameter k led to good performance.

In this paper, a fractional order controller is implemented in conjunction with the LQR algorithm on a fully actuated two story shear building (actuators at each story). Artificial ground accelerations generated by filtered white noise are used as the input excitations in the design phase. Four combinations of FOC and LQR are simulated. To compare the performance of combined LQR-FOC methods with the traditional LQR, these controllers with their optimal parameters are subjected to previously recorded ground motions in addition to the artificial motions used for design. The results obtained demonstrate a considerable achievement in attenuating structural response.

2 Simple Benchmark Civil Structure Model

The deformation response q of structural systems to ground acceleration $\ddot{q}_g$ can be shown by the following system of equations:

$$M\ddot{q} + C\dot{q} + Kq = Eu - Ml\ddot{q}_g \tag{1}$$

where M, C, and K are mass, damping, and stiffness matrices, respectively. E and l are influence vectors (or matrices) due to the applied control force u and the earthquake acceleration $\ddot{q}_g$, respectively. The state-space representation of the above equation is

$$\dot{x} = Ax + Bu + H\ddot{q}_g \tag{2}$$

where the state vector is x = $[q^T \ , \dot{q}^T \ ]^T$, and

$$A = \begin{bmatrix} 0 & I \\ -M^{-1}K & -M^{-1}C \end{bmatrix}, \ B = \begin{bmatrix} 0 \\ M^{-1}E \end{bmatrix}, \text{ and } H = \begin{bmatrix} 0 \\ -l \end{bmatrix} \tag{3}$$

In the above matrices, n denotes the system dimension (number of degrees of freedom)

and m is the number of actuators. Total floor accelerations and relative story drifts are of concern for controlling the structure. Based on (1), these parameters are defined in terms of state variables and control inputs:

$$q_d = \Delta q, \Delta = \begin{bmatrix} 1 & & \\ -1 & 1 & \\ & \ddots & \ddots \\ & -1 & 1 \end{bmatrix} \tag{4}$$

and

$$\ddot{\bar{q}}_t = \ddot{\bar{q}} + l\ddot{\bar{q}}_g = -M^{-1}C\dot{q} - M^{-1}Kq + M^{-1}Eu \tag{5}$$

where q_d and $\ddot{\bar{q}}_t$ represent story drifts and total accelerations, respectively. Equations (4) and (5) are converted to state space representation for outputs, leading to the following simple relationship

$$z = \begin{bmatrix} q_d \\ \ddot{\bar{q}}_t \end{bmatrix} = C_z x + D_z u \tag{6}$$

with Cz and Dz defined as

$$C_z = \begin{bmatrix} \Delta & 0 \\ M^{-1}K & M^{-1}C \end{bmatrix}, D_z = \begin{bmatrix} 0 \\ M^{-1}E \end{bmatrix} \tag{7}$$

3 The Baseline Controller: Weight Optimized Linear Quadratic Regulator

A commonly used performance index for optimal controllers has the form

$$J = \int_0^\tau J_I \, dt, \qquad J_I = x^T Q x + u^T R u + 2x^T N u \tag{8}$$

where R is an m×m positive definite matrix and Q is a 2n×2n weighting matrix such that $Q - NR^{-1}N^T$ is semi-positive definite. To control story drifts and accelerations defined in the output z (6) instead of state variables x, a performance index aimed at attenuating z and u is defined:

$$J'_I = z^T Q z + u^T R u \tag{9}$$

Using the method proposed by Yang et al. [2] leads to the following matrices for (8)

$$Q = C_z^T Q_z C_z, \qquad R = D_z^T R_z D_z + R_z, \qquad N = C_z^T Q_z D_z \tag{10}$$

where Qz and Rz are gain matrices defined for output response and control force. Using the standard linear quadratic (LQR) design with Matlab, we obtain the following full state feedback control law

$$u = -KLQRx \tag{11}$$

where KLQR is the optimal feedback gain matrix obtained using [K,S,E] = LQR(SYS,Q,R,N) in Matlab.

In this work, we wish to establish an optimal baseline performance for comparison to other control schemes. Therefore, an additional parameter optimization procedure is applied to search for a best set of gain matrices Q and R. To simplify the case, diagonal structures of Q and R are assumed. Henceforth, this baseline controller will be referred to as "weight optimized LQR controller."

4 Proposed Fractional Order Control Scheme

4.1 Basic Idea and Definitions. After Newton and Leibniz discovered calculus in the 17th century, fractional-order calculus has been studied as an alternative calculus in mathematics [9,10]. As claimed by Chen et al. [11], fractional order calculus will play an important role in smart mechatronic and biological systems. Recently, in the control field, fractional order dynamic systems and controls have received increasing attention [12–16]. Pioneering works and recent developments in application of fractional calculus to dynamical systems and controls can be found in [17–23]. For a more detailed explanation about fractional dynamics and control, refer to [24] and [25].

Clearly, four variations are relevant for closed-loop control systems: 1) integer order

(IO) plant with IO controller; 2) IO plant with fractional order (FO) controller; 3) FO plant with IO controller and 4) FO plant with FO controller. In control practice, the fractional-order controller is more common, because the plant model may have already been obtained as an integer order model in the classical sense. From an engineering point of view, improving or optimizing performance is the major concern [26]. Hence, our objective is to apply fractional order control (FOC) to enhance the integer order dynamic system performance [21,26].

In this paper, we propose to include a fractional derivative or integral of the state x in the feedback control law similar to (12):

$$u = -K_{LQR}x + K_{FOC}\frac{d^{\alpha}x}{dt^{\alpha}} \tag{12}$$

where KFOC is the gain matrix to be found using optimization procedures.

Several definitions for fractional order derivatives and integrals have been proposed. One of the main issues in applying these definitions is the initialization problem. Lorenzo and Hartley [27,28] have demonstrated that using constants to represent the background history of the subjected function is not an adequate way to handle initialization for fractional differintegral operators. This problem can be solved by introducing an initialization function in which the history of the subjected function plays a major role [27,28]. In seismic control of structures, the history of structure response is unknown and as a result, finding the initialization function is almost impossible. However, the external excitations on the system prior to earthquake or strong winds are usually too small to load the structure to its yield capacity, such that the prior structural response is highly likely to be strictly linear. Also, the random nature of external excitations can be modeled as the output of linear filters, called shaping filters, applied to white noise input

[1,29]. Incorporating these shaping filters into the structure model, a new system with white noise input will be formed. The expected value of the state and output of this linear system with white noise input is theoretically zero. Furthermore, the magnitude of structural response due to dynamic loads on the structure prior to the earthquake is negligible compared to the response of the structure during earthquake. Thus, a good approximation of the history of structural response prior to earthquake is a constant equal to zero. In such cases, different definitions of fractional differintegral operators result in the same solution. The zero prior response approximation may be inaccurate for wind-sensitive structures – tall buildings in windy zones – where the magnitude of structural response is comparable before and during the control period.

In this study, the Caputo definition for a fractional differintegral operator is used in which $\frac{d^{\alpha}x}{dt^{\alpha}}$ is defined as follows [30,31]:

$$\frac{d^{\alpha}x}{dt^{\alpha}} = \frac{1}{\Gamma(\alpha - n)}\int_0^t \frac{x^{(n)}(\tau)d\tau}{(t-\tau)^{\alpha+1-n}} \tag{13}$$

where n is an integer satisfying $n - 1<\alpha<n$ and Γ is the Euler Gamma function. The optimal value of the fractional order α, a real number such that α in $(-1, 1)$, will be explored. Four variants of the FOC-LQR scheme in (12) considered in this paper are as follows:

1) KLQR = 0, KFOC = −KWOLQR

$$u = -K_{WOLQR}\frac{d^{\alpha}x}{dt^{\alpha}} \tag{14}$$

2) KLQR = 0, KFOC determined from optimization

(a) same α for all states

$$u = K_{FOC}\frac{d^{\alpha}x}{dt^{\alpha}} \tag{15}$$

(b) different α for each state

$$u = K_{FOC}\frac{d^{\alpha_i}x}{dt^{\alpha_i}} \tag{16}$$

3) KLQR = KWOLQR, KFOC determined from optimization, (different α for each state)

$$u = -K_{WOLQR}x + K_{FOC}\frac{d^{\alpha_i}x}{dt^{\alpha_i}} \tag{17}$$

where KWOLQR denotes the gain matrix of the weight optimized LQR. Further explanation of the above cases is given in the following sections.

4.2 Modified Oustaloup's Approximation Algorithm. The approximation algorithm presented by Oustaloup et al. [32] is widely used. In this method, a frequency band of interest is considered, within which the frequency domain responses are fit by a bank of integer order filters to the fractional order derivative. For the present study a modification to Oustaloup's approximation method [33,34], which can improve the fitting in the boundary regions is applied. Suppose that the frequency range to be fit is given by [ωA, ωB]. It is easy to show that the term s^{α} can be substituted with

$$K(s) = \left(\frac{1+\frac{s}{\frac{d}{b}\omega_B}}{1+\frac{s}{\frac{b}{d}\omega_H}}\right) \tag{18}$$

where 0<α<1, s = jω, b > 0, d > 0, and

$$K(s) = \left(\frac{bs}{d\omega_B}\right)^{\alpha}\left(1+\frac{-ds^2+d}{ds^2+b\omega_h s}\right)^{\alpha} \tag{19}$$

In the frequency range $\omega_B<\omega<\omega_H$, using the Taylor series expansion

$$K(s) = \left(\frac{bs}{d\omega_B}\right)^{\alpha}\left[1 + \alpha p(s) + \frac{\alpha(\alpha-1)}{2}p^2(s) + \cdots\right] \tag{20}$$

with

$$p(s) = 1 + \frac{-ds^2 + d}{ds^2 + b\omega_h s} \tag{21}$$

the following expression for s^{α} can be obtained

$$s^{\alpha} = \frac{(d\omega_B)^{\alpha} b^{-\alpha}}{\left[1 + \alpha p(s) + \frac{\alpha(\alpha-1)}{2}p^2(s) + \cdots\right]}\left(\frac{1 + \frac{s}{\frac{d}{b}\omega_B}}{1 + \frac{s}{\frac{b}{d}\omega_H}}\right)^{\alpha} \tag{22}$$

Truncating the Taylor series to 1 leads to

$$s^{\alpha} = \frac{(d\omega_B)^{\alpha} b^{-\alpha}}{[1 + \alpha p(s)]}\left(\frac{1 + \frac{s}{\frac{d}{b}\omega_B}}{1 + \frac{s}{\frac{b}{d}\omega_H}}\right)^{\alpha} \tag{23}$$

Compared to Oustaloup's approximation algorithm, the equation given in (23) has one additional component that can overcome the boundary fitting problem. The second component in the right hand side of (23) can be evaluated directly by Oustaloup's method using the zigzag piecewise approximation in the Bode plot.

The above continuous-time approximation is explained in more detail in [33] and a Simulink block is provided and illustrated in [34]. As a side remark, other finite integer order approximation schemes in discrete-time form are available [35]. In this paper, we use the Simulink block for s_ based on modified Oustaloup's approximation from [34].

5 Numerical Example

The structure considered is a two story shear building excited by ground motions at the

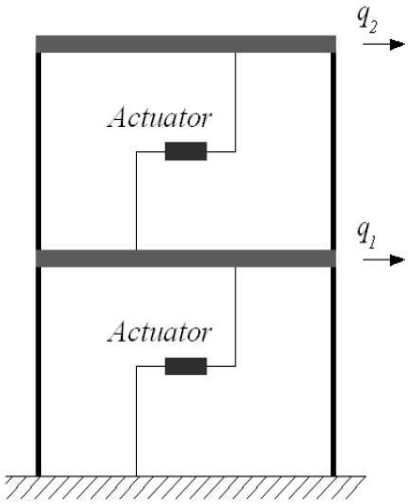

Fig. 1 Schematic view of a simple 2-story structure

base level. A schematic view of the structure together with its degrees of freedom is shown in Fig. 1. Structural mass and stiffness are given in Table 1. Natural periods of the building are 0.3 and 0.14 seconds for the first and second modes, respectively. Rayleigh damping is applied based on 2% damping in each mode. The magnitude of control force applied to the structure is bounded to ±20 kN.

5.1 LQR Weight Optimization Process. One of the biggest issues in implementing optimal controllers is selecting the best gain parameters. The control gain obtained from the LQR algorithm is completely dependent on the objective function defined in (8). Through this index, designers can emphasize attenuation of the structural responses that are of greatest concern. While this index provides intuition to select the pattern for gain

Table 1 Structural parameters

Floor masses (kg)	Stiffness (kN/m)
m_1=6000	k_1=6141
m_2=4000	k_2=3509

matrices, it will not result in an optimal design. Furthermore, the force capacities of both actuators (to apply force) and connections (to which force is exerted) are limited, and as a consequence, the calculated input force should be bounded. This issue also increases the complexity of choosing gain matrices. To solve this problem, a performance criterion different from the one introduced in (8) is proposed:

$$PI = \beta_1 \sum_i \frac{RMS(z_c)}{RMS(z_0)} + \beta_2 \sum_i \frac{Max|z_c|}{Max|z_0|} \tag{24}$$

where z_c and z_0 are the output of the controlled and uncontrolled cases, respectively. The first component emphasizes the mitigation of the root mean square response and the second component the peak response. The parameters β_1 and β_2 in the function give designers the ability to specialize the performance index for specific purposes. For instance, if the aim is to resist against extreme events like earthquakes, peak response rather than RMS response should be reduced or minimized to prevent collapse. However, in windy zones where the occupants comfort level is of greater concern, RMS response would govern design requirements and emphasis can be placed on the first component of the performance index. The objective function defined above (24) is used in an optimization process to find the most appropriate weighting parameters in (8).

The nature of earthquakes is stochastic and a controller designed for only one earthquake record may not give good performance during other earthquakes. To account for this property of the excitation, 64 artificially generated earthquake records are used in the optimization procedure. To produce these records, white noise signals were passed through a Kanai-Tajimi filter [36]. The MATLAB SIMULINK package and Optimization Toolbox were used to simulate the building, controller, and earthquake records. Figure 2 shows the optimization model in SIMULINK.

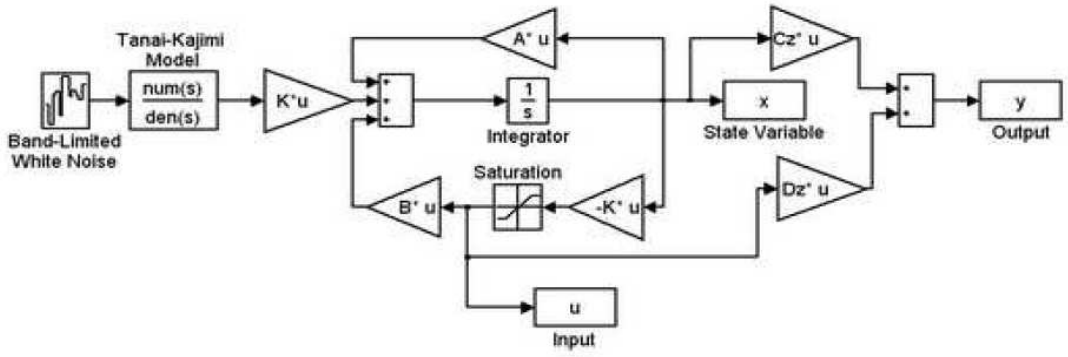

Fig. 2 The Simulink model of the LQR control

In this paper β_1 and β_2 are assumed to be 1 and 2 respectively. The optimization process led to Qz = diag([20.919, 60.993, 8.216e-7, 48.427]) and Rz = diag([6.088e-7, 9.9783e-7]).

5.2 Combined FOC and LQR. As mentioned in previous sections, four general formations for the controller structure are considered. RMS and peak structural responses for each controller type together with the uncontrolled and optimal LQR controlled structures excited by the 64 artificially generated ground motions are presented in Table 2. As expected, response reduction in the optimal LQR controlled structure is significant compared to the uncontrolled case; 67% reduction is achieved in J.

In Case (1) of combined FOC and LQR, the controller is assumed to have only the fractional part, i.e. KLQR = 0, and the input is derived through (14). The gain matrix for α-order state variables, KFOC, is the optimized weight LQR gain matrix KWOLQR and the only parameter to be identified is the fractional order, α. Peak and RMS responses of the structure for different values of α normalized with respect to the comparable optimized LQR responses are shown in Fig. 3. The value of α that minimizes the relative

response varies for different types of response measures and outputs but is generally somewhere between 0 and 0.2 (Fig. 3). Using the objective index in (24), _opt is found to be 0.05. As can be seen, this controller does not result in significant reduction in response compared to the optimized LQR method. This result could have been predicted beforehand, because the only parameter optimized is the order, α, and the weight optimized LQR gain matrix clearly is not the best choice for this case. Thus, reduction in the J factor with respect to the optimized LQR is only 2% (Table 2).

For Case (2a), KFOC is defined from optimization rather than assumed as KWOLQR

Table 2 Root mean squares (RMS) and peak structural responses with their standard deviations for the optimization part

Controller Type	Response Measure	Drift (cm)		Acceleration (g)		J
		1st floor(SD*)	2nd floor(SD)	1st floor(SD)	2nd floor(SD)	
W/O Control	RMS	0.985 (0.148)	0.966 (0.149)	0.464 (0.064)	0.865 (0.134)	12
	Peak	2.976 (0.412)	2.908 (0.425)	1.444 (0.188)	2.602 (0.380)	
LQR	RMS	0.318 (0.019)	0.259 (0.017)	0.179 (0.010)	0.197 (0.013)	3.955
	Peak	1.086 (0.160)	0.896 (0.148)	0.622 (0.080)	0.707 (0.134)	
Case(1)	RMS	0.304 (0.019)	0.250 (0.019)	0.175 (0.010)	0.180 (0.013)	3.889
	Peak	1.061 (0.174)	0.914 (0.171)	0.626 (0.083)	0.687 (0.148)	
Case(2a)	RMS	0.074 (0.014)	0.024 (0.006)	0.155 (0.010)	0.154 (0.010)	2.517
	Peak	0.615 (0.143)	0.236 (0.105)	0.608 (0.105)	0.633 (0.145)	
Case(2b)	RMS	0.075 (0.015)	0.022 (0.006)	0.155 (0.010)	0.157 (0.010)	2.496
	Peak	0.616 (0.144)	0.213 (0.113)	0.605 (0.104)	0.629 (0.143)	
Case(3)	RMS	0.108 (0.008)	0.059 (0.006)	0.175 (0.009)	0.153 (0.008)	2.754
	Peak	0.552 (0.092)	0.353 (0.092)	0.658 (0.067)	0.658 (0.144)	

*SD stands for standard deviation.

(15). Since KFOC is 2 × 4, 9 parameters must be found in an optimization process. Simulation results show large improvements in responses where J is reduced by 36% with respect to the optimized LQR method. In particular, story drifts are reduced significantly. Story drifts in the first and second stories are reduced by 77% and 91% for RMS drift and 43% and 76% for peak drift, respectively (Table 2). Although mitigation of acceleration response is not as significant as for drift, a considerable reduction is still seen. Accelerations in the first and second floor are reduced by 13% and 10% for RMS acceleration and 2% and 10% for peak acceleration, respectively (Table 2).

In Case (1) and Case (2a), the order α was considered to be the same for all state variables. In the controller configuration for Case (2b), different values of α are assigned for each state variable; hence three extra variables are added to the system. Case (2b) results in relatively similar performance to the previous Case (2a) where the same order was used for all state variables. The objective index J is reduced by 37% relative to the optimized LQR method, compared to 36% for the controller of Case (2a) (Table 2). Therefore, the increased computational complexity to identify different fractional orders for the state variables introduces only marginal benefit.

In Case (3), a fractional order controller is added to the weight optimized LQR, i.e. KLQR = KWOLQR, and the gain matrix for the fractional part and the orders of state variables are found through optimization. In this case, J is reduced by 30% with respect to the weight optimized LQR method, showing less improvement compared to Case (2a) and Case (2b).

A graphical representation of the results of Table 2 is given in Fig. 4. Comparing the responses of the uncontrolled and controlled structures reveals the effectiveness of

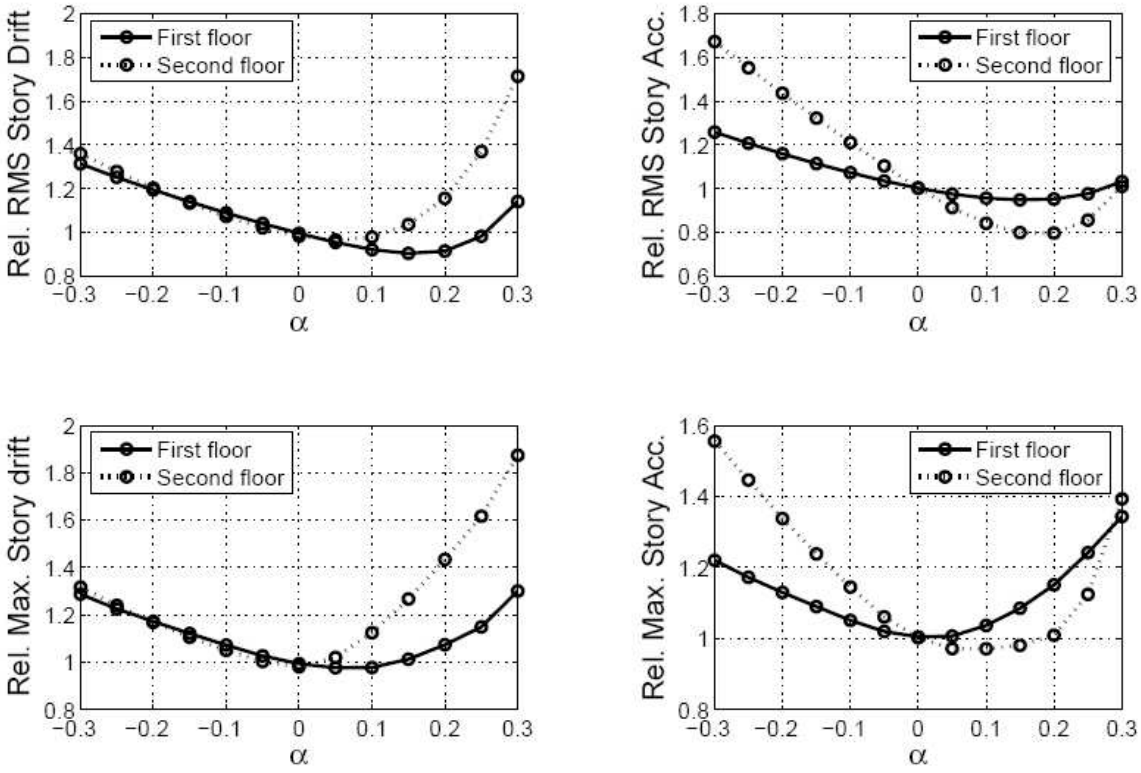

Fig. 3 Relative response of the case 1 controller

various control techniques in mitigating structural response during earthquakes. Introducing fractional order filters into the controller structure reduces considerably the inter-story drift response for both the peak and RMS measures, but reduces only slightly the acceleration response. Case (2a) and Case (2b) perform similarly and give the largest response reduction (Fig. 4).

5.3 Simulation Results for Real Ground Motions. To observe the performance of the various controllers introduced here to realistic excitation, the building structure is subjected to the following previously recorded ground motions with peak ground accelerations (PGA) as listed: 1940 El Centro at Imperial Valley (PGA 0.3129 g), 1995 Kobe at Japanese Meteorological Agency (PGA 0.8213 g), and 1994 Northridge at

Sylmar (PGA 0.8433 g). The gain matrices and fractional state variables, found from the optimization processes in the previous section, are applied to the controllers. Simulation results are presented in Table 3.

The response trends for realistic ground motions are similar to those produced by optimization, which verifies the procedure used to obtain the best parameters for the gain matrix and/or the order of state variables. According to the results presented in Table 2 based on the 64 artificially generated ground motions, the objective index and almost all response measures for case (3) are larger than the corresponding values for cases (2a) and (2b). This trend is also reflected in structural responses to the El Centro earthquake in Table 3; that is, the case (2b) controller gives the best response, and the performance index for case (3) is 36% larger. However, the case (3) controller gives the best response and the lowest objective index for the Kobe and Northridge motions.

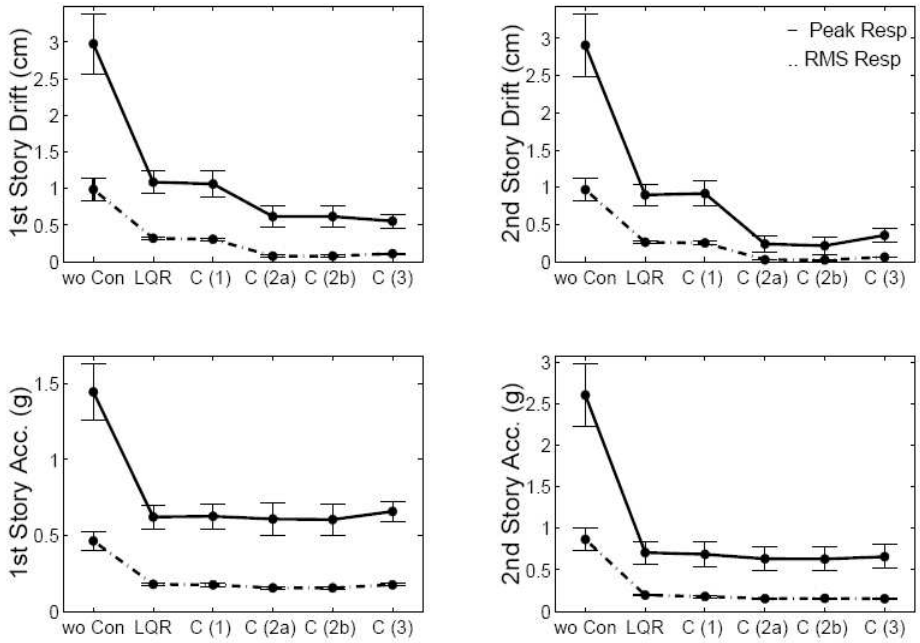

Fig. 4 Structural performance of the building for different controllers subjected to artificially generated ground motions

Table 3 Root mean squares (RMS) and peak structural responses

Controller Type	Earthquake	Drift (cm)				Acceleration (g)				
		1st floor		2nd floor		1st floor		2nd floor		
		RMS	Peak	RMS	Peak	RMS	Peak	RMS	Peak	J
W/O Control	ElCentro	0.287	1.206	0.287	1.317	0.143	0.771	0.256	1.182	12
	Kobe	0.533	2.82	0.493	2.469	0.269	1.472	0.441	2.207	12
	Northridge	0.829	4.695	0.81	3.873	0.391	2.598	0.725	3.462	12
LQR	ElCentro	0.108	0.676	0.084	0.494	0.062	0.366	0.064	0.367	4.795
	Kobe	0.347	2.223	0.301	1.843	0.183	1.191	0.227	1.536	8.534
	Northridge	0.314	3.264	0.288	2.832	0.161	1.755	0.225	2.363	7.026
Case(1)	ElCentro	0.107	0.695	0.084	0.523	0.061	0.44	0.06	0.367	5.035
	Kobe	0.349	2.287	0.313	1.985	0.182	1.274	0.226	1.547	8.841
	Northridge	0.324	3.368	0.306	3.003	0.164	1.849	0.233	2.404	7.306
Case(2a)	ElCentro	0.011	0.228	0.004	0.088	0.055	0.36	0.054	0.351	2.69
	Kobe	0.172	1.148	0.093	0.981	0.17	1.221	0.185	1.381	6.084
	Northridge	0.164	2.196	0.115	1.637	0.142	1.497	0.166	1.972	5.004
Case(2b)	ElCentro	0.011	0.234	0.004	0.071	0.055	0.36	0.055	0.336	2.645
	Kobe	0.18	1.246	0.099	1.053	0.175	1.407	0.194	1.45	6.594
	Northridge	0.168	2.185	0.117	1.723	0.144	1.749	0.169	2.054	5.303
Case(3)	ElCentro	0.037	0.278	0.02	0.256	0.069	0.492	0.058	0.331	3.594
	Kobe	0.168	1.194	0.109	0.977	0.171	1.05	0.174	1.381	5.881
	Northridge	0.166	2.267	0.124	1.531	0.147	1.545	0.16	1.868	4.977

Results also indicate that the relative reduction in response achieved during the El Centro earthquake is much more than that obtained in the Kobe and Northridge earthquakes. Although artificial records generated by the Kanai-Tajimi filter in the optimization procedure have power spectral density curves relatively close to real ground motions, their pattern in time domain could be much different. In this sense, the artificial records used for optimization are apparently more representative of the El Centro record than of the Northridge or Kobe record. Furthermore, the PGAs of the Northridge and Kobe records, which are roughly 2.5 times the PGA of the El Centro records, lead to greater demands on the amplitude of the input force. As mentioned previously, an upper

and lower bound is placed on the control force to account for actuator and joint capacities. These bounds prevent controllers from applying the theoretically desired forces, which leads to substantial degradation of the efficiency of the control system when the difference between the desired and applied forces is considerable.

6 Conclusion And Future Research Efforts

The application of fractional order filters in conjunction with an LQR controller has been introduced in this paper. Several combinations of FOC and LQR were considered and subjected to optimization to find the most appropriate parameters. 64 artificially generated earthquakes were used to optimize the controller gains. Simulation results demonstrated that introducing the fractional order filter into the LQR controller led to a great advance in attenuating the response over optimized LQR alone. The best performance was produced when a single fractional order was assigned to all state variables and the gain matrix was found from optimization. Considering distinct fractional orders for each state variable did not appreciably improve the performance, and in some cases induced a higher structural response. Simulating the system with actual recorded ground motions led to the same trends for response attenuation, implying that the optimization process works well.

To develop a simple model with which to apply proposed controller, the structure has been assumed to be fully observable. However, this assumption is far from realistic and considering noise effects will degrade the efficiency of controllers. Next, the performance of the proposed controllers should be assessed in a more realistic setting, where observer-based controllers are designed based on filtered noise measurements. Also, dynamics of actuators, nonlinearity in the system due to plastic deformation of

structural elements, and time delay are some of the issues that have not yet been investigated and should be addressed in future research.

References

[1] Soong, T. T., 1990, *Active Structural Control: Theory and Practice,* Longman Scientific and Technical, Essex, England.

[2] Yang, J. N., Li, Z., and Vongchavalitkul, S., 1994, "Generalization of Optimal Control Theory: Linear and Nonlinear Control," J. Eng. Mech., **120**, pp. 266-283.

[3] Chang, C. C., and Henry, T. Y., 1994, "Instantaneous Optimal Control of Building Frames," J. Struct. Eng. **120**, pp. 1307-1325.

[4] Ankireddi, S., and Yang, H. T. Y., 1997, "Multiple Objective LQG Control of Wind-Excited Buildings," J. Struct. Eng., **123**, pp. 943-951.

[5] Guoping, C., and Jinzhi, H., 2002, "Optimal Control Method for Seismically Excited Building Structures with Time-Delay in Control," J. Eng. Mech., **128**, pp. 602-612.

[6] Ramallo, J. C., Johnson, E. A., and Spencer. Jr., B. F., 2002, "Smart Base Isolation Systems," J. Eng. Mech. **128**, pp. 540-551.

[7] Adeli, H., and Kim, H., 2004, "Wavelet-hybrid Feedback Least Mean Square Algorithm for Robust Control of Structures," J. Struct. Eng. **130**, pp. 128-137.

[8] Wang, S. G., 2004, "Linear Quadratic Gaussian-alpha Control with Relative Stability and Gain Parameter for the Structural Benchmark Problems," J. Eng. Mech., **130**, pp. 511-517.

[9] Debnath, L, 2004, "A Brief Historical Introduction to Fractional Calculus," Int. J. Math. Educ. Sci. Technol. **35(4)**, pp. 487-501.

[10] Magin, R. L., 2004, "Fractional Calculus in Bioengineering," Crit. Rev. in Biomed.

Eng. **32**, pp. 1-377.

[11] Chen, Y., Xue, D., and Dou, H., 2004, "Fractional calculus and biomimetic control," *Proceedings of the First IEEE International Conference on Robotics and Biomimetics (RoBio04)*, IEEE, Shengyang, China, pp. 901-906.

[12] Lurie, B. J., 1994, "Three-parameter tunable tilt-integral-derivative (TID) controller," U.S. Patent No. 5,371,670.

[13] Podlubny, I., 1999, "Fractional-order Systems and PID Controllers," IEEE Trans. Autom. Control, **44**, pp. 208-214.

[14] Oustaloup, A., Mathieu, B., and Lanusse, P., 1995, "The CRONE Control of Resonant Plants: Application to a Flexible Transmission," Eur. J. of Control, **1**, pp. 113-121.

[15] Oustaloup, A., Moreau, X., and Nouillant, M., 1996, "The CRONE Suspension," Control Eng. Pract., **4**, pp. 1101-1108.

[16] Raynaud, H., and Zerga¨ınoh, A., 2000, "State-space Representation for Fractional Order Controllers," Automatica **36**, 1017-1021.

[17] Manabe, S., 1960, "The Non-integer Integral and Its Application to Control Systems," JIEE (Japanese Institute of Electrical Engineers) Journal **80**, pp. 589-597.

[18] Manabe, S., 1961, "The Non-integer Integral and Its Application to Control Systems," ETJ of Japan, **6**, pp. 83-87.

[19] Oustaloup, A., 1981, "Fractional Order Sinusoidal Oscilators: Optimization and Their Use in Highly Linear FM Modulators," IEEE Trans. Circuits and Syst., **28**, pp. 1007-1009.

[20] Axtell, M., and Bise, E. M., "Fractional calculus applications in control systems,"

Proceedings of the IEEE 1990 National Aerospace and Electronics Conference, New York, pp. 563–566.

[21] Vinagre, B. M., and Chen, Y., 2002, "Lecture notes on fractional calculus applications in automatic control and robotics," *The 41st IEEE CDC2002 Tutorial Workshop No. 2*, Las Vegas, NV, pp. 1–310 (URL: http://mechatronics.ece.usu.edu /foc/cdc02 tw2 ln.pdf).

[22] Tenreiro Machado, J. A. (Guest Editor), 2002, "Special Issue on Fractional Calculus and Applications," Nonlinear Dyn., **29**, pp. 1-385.

[23] Ortigueira, M. D., and Tenreiro Machado, J. A. (Guest Editors), 2003, "Special Issue on Fractional Calculus and Applications," Signal Process., **83**, pp. 2285-2480.

[24] Xue, D., and Chen, Y. Q., "A comparative introduction of four fractional order controllers," *Proceedings of the 4th IEEE World Congress on Intelligent Control and Automation (WCICA02),* IEEE, Shanghai, China, pp. 3228–3235.

[25] Chen, Y. Q., 2006, "Ubiquitous fractional order controls?," *Proceedings of the Second IFAC Symposium on Fractional Derivatives and Applications (IFAC FDA06),* Porto, Portugal, July 19-21, pp. 1-12.

[26] Xue, D., Zhao, C. N., and Chen, Y. Q., 2006, "Fractional order pid control of a dc-motor with an elastic shaft: a case study," *Proceedings of American Control Conference*, Minneapolis, MN, pp. 3182–3187.

[27] Lorenzo, C. F., and Hartley, T. T., 2000, "Initialized Fractional Calculus," Int. J. of Appl. Math., **3**, pp. 249-265.

[28] Lorenzo, C. F., and Hartley, T. T., "Initialization of fractional differential equations: background and theory," *International Design Engineering Technical*

Conferences/Computers and Information in Engineering Conference (IDETC/CIE 2007), ASME, Las Vegas.

[29] Crandall, S. H., and Mark, W. D., 1963, *Random Vibration in Mechanical Systems*, Academic, New York.

[30] Caputo, M., 1967, "Linear models of dissipation whose q is almost frequency independent-II," Geophys. J. R. Astron. Soc. **13**, pp. 529-539.

[31] Podlubny, I., 1999, *Fractional Differential Equations,* Academic, New York.

[32] Oustaloup, A., Levron, F., Nanot, F., and Mathieu, B., "Frequency Band Complex Non Integer Differentiator: Characterization and Synthesis," IEEE Trans. Circuits Syst., I: Fundam. Theory Appl., **47**, pp. 25-40.

[33] Xue, D., Zhao, C. N., and Chen, Y. Q., 2006, "A modified approximation method of fractional order system," *Proceedings of 2006 IEEE Conference on Mechatronics and Automation*, Luoyang, China, pp. 1043–1048.

[34] Xue, D., and Chen, Y. Q., 2007, *Solving Control Related Mathematic Problems in Matlab,* Tsinghua University Press, Beijing, China.

[35] Chen, Y. Q., Vinagre, B. M., and Podlubny, I., 2004, "Continued Fraction Expansion Approaches to Discretizing Fractional Order Derivatives: an Expository Review," Nonlinear Dyn., **38**, pp. 155-170.

[36] Soong, T. T., and Grigoriu, M., 1993, *Random Vibration of Mechanical and Structural Systems,* Prentice Hall, Englewood Cliffs, NJ.

CHAPTER III

ROBUST STABILITY AND PERFORMANCE OF FILTER ENHANCED H_2/LQG CONTROLLERS FOR NONLINEAR STRUCTURES

Abdollah Shafieezadeh and Keri L. Ryan[2]

SUMMARY

This study illustrates the application of frequency dependent filters to improve the effectiveness of active control systems designed to mitigate the seismic response of large scale civil structures. These filters are introduced as band pass pre-filters to the optimally designed H_2/LQG controller to reduce the maximum singular value response of input-output transfer matrices over a defined frequency range. Furthermore, a structured uncertainty model is proposed to evaluate robustness of stability and performance considering nonlinear force-deformation behavior of structures. The proposed perturbation model characterizes variations in the stiffness matrix more accurately; thereby reducing over-conservatism in the estimated destabilizing perturbations. The aforementioned techniques are applied to the nonlinear SAC 3-story steel building. Numerical results indicate that introducing filters can enhance the performance of the system in almost all response measures, while preserving robustness of stability and performance.

1. INTRODUCTION

Enhanced performance objectives for the seismic response of civil structures in

[2] Coauthored by Abdollah Shafieezadeh and Keri Ryan.

large earthquakes are increasingly targeted to avoid large economic losses associated with damage in structural and nonstructural components. Substantially improved performance can be achieved through the application of structural control methods, and the last two decades have led to major accomplishments in the development of control devices and algorithms to enhance the performance of structures [1, 2]. Optimal control theories have been shown to be effective for civil structures. When the structure is fully observed, linear quadratic regulators (LQR) are very powerful in disturbance rejection and have guaranteed robust stability properties [3]. Numerous applications of LQR and linear quadratic Gaussian (LQG) methods in structural control have been proposed, e.g. [4-7]. As evidence of the preeminence of LQR and LQG methods, they are typically the baseline controllers against which new approaches are judged [8-12], and a number of investigations have focused exclusively on enhancing these methodologies to improve system performance in the time domain [13-15].

In seismic control applications, characteristics of the input ground acceleration disturbance to the system, represented by its power spectrum, cannot be accurately captured over all frequencies by static filters such as the Kanai-Tajimi filter [16]. A limited number of studies have introduced frequency domain techniques to enhance LQR/LQG controller performance. Frequency dependent weighting functions were applied to the input excitation and regulated outputs in place of constant weighting matrices in LQG control method [17, 18]. Min et al. [19] extended the weighting functions to sensor noise and demonstrated experimental results to verify the satisfactory performance of frequency domain optimal control design methods. Further improvements in response may be possible by using filters to adjust the frequency

content of the input disturbance used to design the controller.

Unlike the LQR method, robustness of the LQG approach to uncertainties is not guaranteed [20] and the control design should be checked for robustness for each specific application. Uncertainties in modeling large scale structures result from imprecise information on system properties (e.g. mass, damping, and stiffness matrices) and input disturbances; and are compounded by the complex behavior of structures that respond in their nonlinear range. Perturbations techniques have been applied to check robustness of stability and performance, where uncertainty in system properties were represented by unstructured perturbation matrices [21-23] or block diagonal perturbation matrices [24-27] for mass, damping, and stiffness. In the block diagonal approach, each diagonal matrix is still an unstructured perturbation matrix. However, even more accurate results are achievable if structured uncertainty models are utilized for each of the perturbation matrices in the global block diagonal uncertainty model.

The goals of this investigation are: (1) to improve the performance of optimally designed H_2/LQG controllers using band pass pre-filters, which provide the flexibility to shape the frequency response of input-output transfer matrices, thereby reducing their maximum singular value response over the frequencies of concern; and (2) to present a general approach using structured perturbation theory to verify robustness of stability and performance of nonlinear structures. The structured perturbation model quantifies the stiffness variations induced by nonlinear force-deformation behavior of structural elements, and applies these variations as bounded structured uncertainties to the model stiffness matrix.

2. SYSTEM MODEL AND REFERENCE H_2/LQG CONTROLLER

An optimal H_2/LQG controller is designed to serve as a baseline against which to assess filter enhancements. The design techniques described are applicable to any civil structure with an active control system that includes dynamic actuators for control forces and sensors for observers. The H_2/LQG controller is known to be optimal for a linear structure initially at rest. While the structural response may be nonlinear in a large seismic event, this nonlinearity can be minimized through an effective active control system. Therefore, the controller is designed based on the H_2/LQG strategy, and nonlinear behavior is indirectly accounted for through numerical optimization.

The governing equations of a structure subjected to earthquake ground acceleration, assuming the system remains linear, are as follows

$$\mathbf{M}_0\ddot{\mathbf{x}} + \mathbf{C}_0\dot{\mathbf{x}} + \mathbf{K}_0\mathbf{x} = \mathbf{E}_u\mathbf{u} - \mathbf{M}_0\mathbf{E}_g\ddot{\mathbf{x}}_g \tag{1}$$

where vectors $\mathbf{x}$ and $\mathbf{u}$ contain the relative story displacements and input control forces, respectively, and $\ddot{\mathbf{x}}_g$ contains the earthquake ground acceleration. $\mathbf{M}_0$, $\mathbf{C}_0$, and $\mathbf{K}_0$ are the nominal mass, damping and stiffness matrices of the structure, and $\mathbf{E}_g$ and $\mathbf{E}_u$ are influence matrices mapping the input ground acceleration and applied control forces to the displacement degrees of freedom. Absolute acceleration responses at story levels are measured as feedback to the controller. The state-space representation of this system in the linear state with defined inputs $\mathbf{u}_t = <\ddot{\mathbf{x}}_g \ \mathbf{u}^T>^T$ and measured outputs (story accelerations) $\mathbf{y}_m$ is

$$\dot{\mathbf{z}} = \mathbf{A}\mathbf{z} + \mathbf{B}_t\mathbf{u}_t \tag{2a}$$

$$\mathbf{y}_m = \mathbf{C}_m \mathbf{z} + \mathbf{D}_m \mathbf{u}_t + \boldsymbol{\nu} \tag{2b}$$

where

$$\mathbf{z} = \begin{Bmatrix} \mathbf{x} \\ \dot{\mathbf{x}} \end{Bmatrix}, \ \mathbf{A} = \begin{bmatrix} \mathbf{0} & \mathbf{I} \\ -\mathbf{M}_0^{-1}\mathbf{K}_0 & -\mathbf{M}_0^{-1}\mathbf{C}_0 \end{bmatrix}, \ \mathbf{B}_t = \begin{bmatrix} \mathbf{0} & \mathbf{0} \\ -\mathbf{E}_g & \mathbf{M}_0^{-1}\mathbf{E}_u \end{bmatrix} \tag{3a}$$

$$\mathbf{C}_m = \begin{bmatrix} -\mathbf{M}_0^{-1}\mathbf{K}_0 & -\mathbf{M}_0^{-1}\mathbf{C}_0 \end{bmatrix}, \ \mathbf{D}_m = \begin{bmatrix} \mathbf{0} & \mathbf{M}_0^{-1}\mathbf{E}_u \end{bmatrix} \tag{3b}$$

The index *m* represents measured responses and ν is the measurement noise.

Optimal H_2/LQG control methods minimize the average linear system response and control force in the form of a time cumulative performance index. Traditionally, the objective function for the performance index *J* of a system with *n* degrees of freedom and *r* controllers has the following form:

$$J = \int_0^{t_f} \left(\mathbf{x}^{\mathrm{T}} \mathbf{Q} \mathbf{x} + \mathbf{u}^{\mathrm{T}} \mathbf{R} \mathbf{u} + 2\mathbf{x}^{\mathrm{T}} \mathbf{N} \mathbf{u} \right) \ dt \tag{4}$$

where **R** is an *r* by *r* positive definite matrix and **Q** is a 2*n* by 2*n* weighting matrix such that $\mathbf{Q}\text{-}\mathbf{N}\mathbf{R}^{-1}\mathbf{N}^{\mathrm{T}}$ is semi-positive definite.

The Kanai-Tajimi filter [16] is frequently used to approximate the average power spectral density (PSD) of typical ground motions. Earthquake accelerations to the structure are modeled in the control design phase by passing a white noise signal through the Kanai-Tajimi filter, which has the following transfer function.

$$W_{\mathrm{K-T}} = \frac{2\zeta_g \omega_g s + \omega_g^2}{s^2 + 2\zeta_g \omega_g s + \omega_g^2} \tag{5}$$

This transfer function represents the total acceleration response of a single degree of freedom (SDOF) system with natural frequency ω_g and damping ζ_g to an input white noise. These parameters can be adjusted based on the earthquake magnitude, ground resonant frequency, and attenuation of seismic waves.

In the low frequency range, the magnitude of the PSD of real ground motions decreases with decreasing frequency, but the Kanai-Tajimi filter cannot capture this trend. Implementing another second order filter [28] can improve the ground acceleration model in the low frequency range. The corrective filter is defined as

$$W_{\text{cor}} = \frac{s^2}{s^2 + 2\zeta_p \omega_p s + \omega_p^2} \tag{6}$$

Appending this shaping filter to the Kanai-Tajimi filter, the transfer function from input white noise to ground acceleration is

$$W_{\ddot{x}_g w} = W_{\text{cor}} W_{\text{K-T}} \tag{7}$$

Performance objectives are often imposed on a combination of state variables and control forces, known as regulated outputs. Here, the control system is designed to minimize story drifts $\mathbf{x}_{\text{drift}}$ (structural damage) and absolute accelerations $\ddot{\mathbf{x}}_{\text{abs}}$ (nonstructural damage), while at the same time limiting the required force demands $\mathbf{u}$ on the controllers. Based on the linear model (Equation (1)), the regulated outputs $\mathbf{y}_{\text{reg}} = \left\langle \mathbf{x}_{\text{drift}}{}^{\text{T}} \quad \ddot{\mathbf{x}}_{\text{abs}}{}^{\text{T}} \quad \mathbf{u}^{\text{T}} \right\rangle^{\text{T}}$ are accessible through

$$\mathbf{y}_{\text{reg}} = \mathbf{C}_{\text{reg}} \mathbf{z} + \mathbf{D}_{\text{reg}} \mathbf{u}_t \tag{8a}$$

$$\mathbf{C}_{\text{reg}} = \begin{bmatrix} \mathbf{H}_{\text{rel}} & \mathbf{0} \\ -\mathbf{M}_0^{-1}\mathbf{K}_0 & -\mathbf{M}_0^{-1}\mathbf{C}_0 \\ \mathbf{0} & \mathbf{0} \end{bmatrix},\ \mathbf{D}_{\text{reg}} = \begin{bmatrix} \mathbf{0} & \mathbf{0} \\ \mathbf{0} & \mathbf{M}_0^{-1}\mathbf{E}_u \\ \mathbf{0} & \mathbf{I} \end{bmatrix},\ \mathbf{H}_{\text{rel}} = \begin{bmatrix} 1 & & & 0 \\ -1 & 1 & & \\ & \ddots & \ddots & \\ 0 & & -1 & 1 \end{bmatrix}_{n\times n}$$

(8b)

Introducing weighting or gain matrices $\mathbf{Q}_y$ and $\mathbf{R}_y$, the performance index in terms of regulated outputs can be represented by

$$J = \int_0^{t_f} \left(\mathbf{y}_{\text{reg}}{}^{\text{T}} \begin{bmatrix} \mathbf{Q}_y & \mathbf{0} \\ \mathbf{0} & \mathbf{R}_y \end{bmatrix} \mathbf{y}_{\text{reg}} \right) \ dt \tag{9}$$

Equation (9) is a specialization of Equation (4) with

$$\mathbf{Q} = \mathbf{C}_{\text{reg}}{}^{\text{T}}\mathbf{Q}_y\mathbf{C}_{\text{reg}},\ \mathbf{R} = \mathbf{D}_{\text{reg}}{}^{\text{T}}\mathbf{Q}_y\mathbf{D}_{\text{reg}} + \mathbf{R}_y,\ \mathbf{N} = \mathbf{C}_{\text{reg}}{}^{\text{T}}\mathbf{Q}_y\mathbf{D}_{\text{reg}} \tag{10}$$

Gain matrices $\mathbf{Q}_y$ and $\mathbf{R}_y$ (Equations (9) and (10)) are found through a numerical optimization procedure. The following form is selected for these matrices:

$$\mathbf{Q}_y = diag\left(\left[\mathbf{x}_{\text{rms}}{}^{\text{p}}, \alpha_1 \ddot{\mathbf{x}}_{\text{rms}}{}^{\text{p}} \right] \right),\quad \mathbf{R}_y = \alpha_2 . diag\left(\begin{bmatrix} 1 & \cdots & 1 \end{bmatrix} \right) \tag{11}$$

where $\mathbf{x}_{\text{rms}}$ and $\ddot{\mathbf{x}}_{\text{rms}}$ are the root-mean-square (RMS) drift and absolute acceleration response of the uncontrolled structure. Parameters α_1, α_2, and p provide partial control on the relative magnitude of the elements of the gain matrices $\mathbf{Q}_y$ and $\mathbf{R}_y$. Optimizing the gain matrices for large earthquakes that induce nonlinear structural response may reduce the controller effectiveness under linear response in a moderate earthquake, which is judged to be an acceptable tradeoff.

3. ENHANCING CONTROLLER PERFORMANCE USING FILTERS

Despite the improvement offered by the second shaping filter, the Kanai-Tajimi filter is somewhat ineffective in capturing accurately the major characteristics of ground motions, e.g. maximum power, dominant frequency, and bandwidth. The PSD response of the Kanai-Tajimi filter with corrective filter is compared to the PSD of several recorded ground accelerations in Figure 5. The PSD of real ground motions differ substantially from the representative Kanai-Tajimi filter (Figure 5) in the frequency range of 0.5 Hz to 15 Hz. As this frequency range typically includes the fundamental frequency of the linear structure and the strongest ground accelerations, the associated

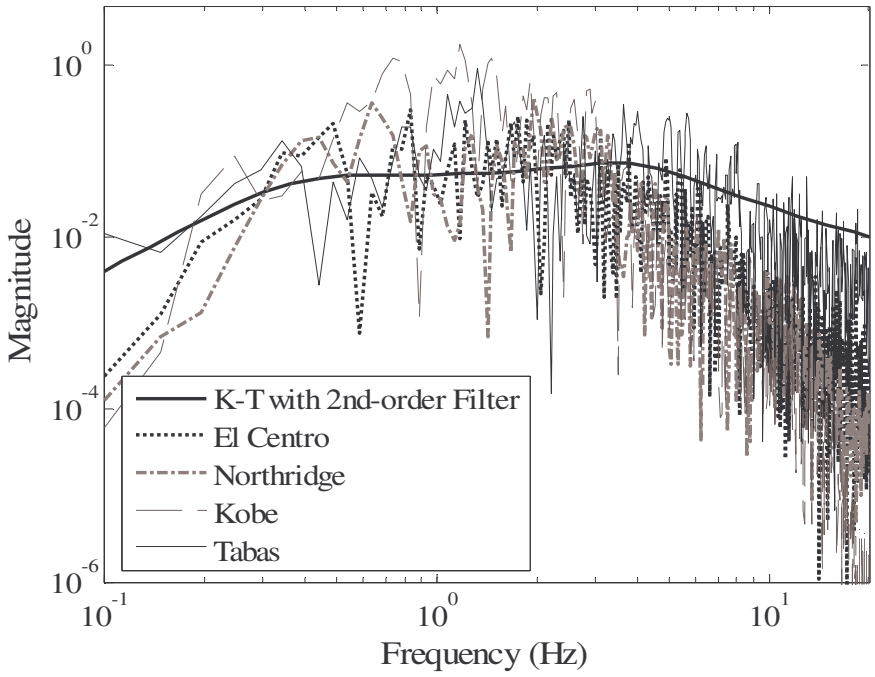

Figure 5. The PSD of Kanai-Tajimi filter with corrective shaping filter (Equation (7)) compared to PSD of the following recorded earthquake accelerations: 1940 El Centro at Imperial Valley Sta. (PGA, 0.461 g), 1994 Northridge at Sylmar Sta. (PGA, 0.569 g), 1995 Kobe at JMA Kobe Sta. (PGA, 1.282 g), and 1974 Tabas at Tabas Sta. (PGA, 0.809 g).

frequency response of input-output transfer matrices over this frequency range may influence the total response of the structure and the overall performance of the controller.

Based on Bode's sensitivity integral, if the open loop transfer function is stable, then

$$\int_0^\infty \ln\left|\mathbf{S}(j\omega)\right| d\omega = 0 \tag{12}$$

where **S** is the sensitivity matrix of the closed loop system [29, 30]. Equation (12) implies that magnitudes of $\mathbf{S} < 1$ over some frequencies must be balanced by magnitudes > 1 over other frequencies, referred to as the water bed effect [30]. A pre-filter W_{pre} to the controller (Figure 6) changes the shape of the maximum singular value (SV) response of an input-output transfer matrix. Based on the water bed effect, pre-filters are strategically applied to reduce the maximum SV response of transfer matrices over the frequencies that contribute most to the response. Although the transfer matrices represent the linear state of the structure in contrast to the expected nonlinear behavior, an effective controller will minimize inelastic response such that the response of transfer matrices is close to the actual response.

Several filter shapes, e.g. low pass filters, high pass filters, and band pass filters, can be considered. The more general band pass filter is derived by multiplying a low and high pass filter together to obtain:

$$W_{\text{bp}} = \frac{s^2 + (l+h)s + lh}{c\left(s^2 + a(l+h)s + blh\right)} \tag{13}$$

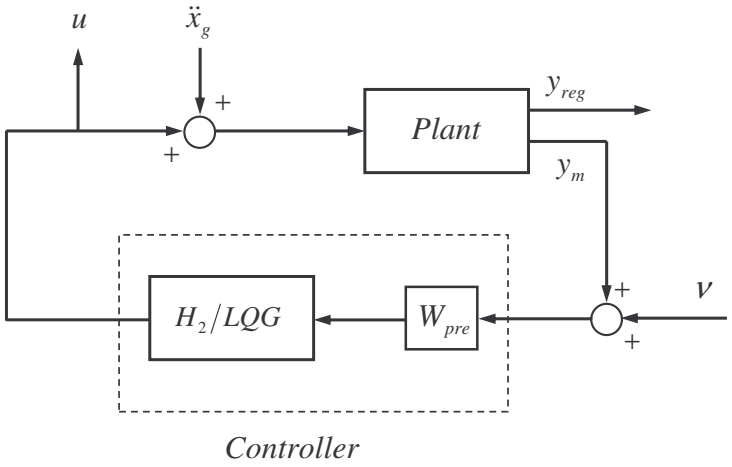

Figure 6. Schematic diagram of the structure, controller and pre-filter.

where l and h represent the low and high transition frequencies, and a, b, and c are scaling coefficients. When $b = 1$, the peak magnitude $|W_{bp}|$ of the filter and the frequency f_p at which it occurs, is

$$\left|W_{bp}(f_p)\right| = -20.\log_{10}(ac) \quad dB, \; f_p = \sqrt{l.h} \quad rad/\sec \tag{14}$$

As the pre-filters aim to mitigate frequency response over a relatively narrow range (0.5 to 15 Hz), a narrow band width is imposed by setting $h=l+1$. Figure 3 illustrates the effect of parameter variation on filter response in the Laplace domain: a controls the magnitude of the filter over the band pass region (Figure 7(a)), b controls the magnitude of the filter at low frequencies (Figure 7(b)), and c controls the filter magnitude over all the frequencies uniformly (Figure 7(c)). Finally, l translates the filter along the frequency axis (Figure 7(d)). Thus, through these four parameters, almost every characteristic of the band pass filter can be controlled.

4. ROBUST STABILITY AND PERFORMANCE

Since the H_2/LQG control approach is based on the linear state of the system at rest, the controller stabilizes the structure in the linear state, but the system is not guaranteed to remain stable or have satisfactory performance when it responds nonlinearly. In the approach outlined here, the whole system (structure with controller) is examined for robust stability and robust performance by treating nonlinearities as uncertainties in the system [30, 31].

Several approaches have been proposed to investigate robust stability and performance of systems [30]. Structured singular value analysis (μ analysis) requires that

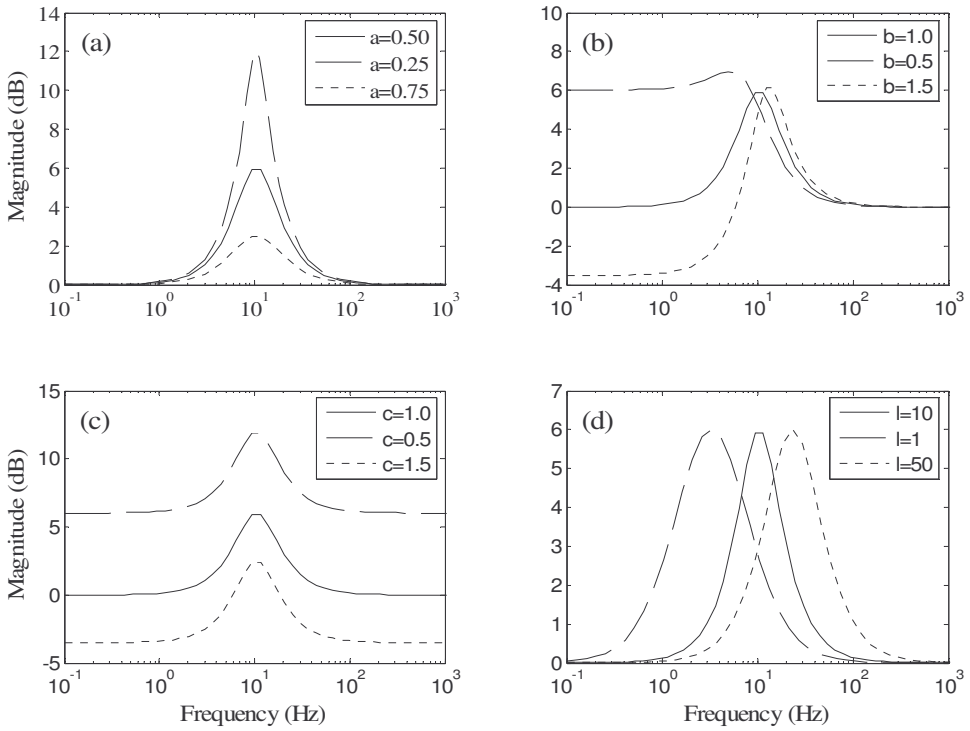

Figure 7. Influence of variation of parameters (a) *a*, (b) *b*, (c) *c*, (d) *l* on the magnitude of the band pass filter, with respect to a reference (solid line) filter with *a*=2, *b*=1, *c*=1, and *l*=10.

observed perturbations to the system are less than the smallest destabilizing perturbation matrix quantified by maximum SV. Under structured uncertainties, μ analysis leads to larger bounds on the destabilizing perturbation matrix and is therefore less overconservative.

The following two theorems are the basis for μ analysis. Assume the system transfer matrix $\mathbf{G}_P$ is a stable, real-rational, proper matrix with the following structure (Figure 8)

$$\mathbf{G}_P = \begin{bmatrix} \mathbf{G}_{11} & \mathbf{G}_{12} \\ \mathbf{G}_{21} & \mathbf{G}_{22} \end{bmatrix} \tag{15}$$

where $\mathbf{G}_{11}$ has M_1 inputs and N_1 outputs and $\mathbf{G}_{22}$ has M_2 inputs and N_2 outputs.

Theorem 1[30] (Robust Stability): *Let $\beta>0$. The loop shown in Figure 8 is well-posed and internally stable for all perturbation matrices $\boldsymbol{\Delta} \in \mathbf{M}(\boldsymbol{\Lambda})$ with $\|\boldsymbol{\Delta}\|_\infty < \frac{1}{\beta}$ if and only if*

$$\sup_{\omega \in \Re} \mu_{\boldsymbol{\Lambda}}(\mathbf{G}_{11}(j\omega)) \le \beta \tag{16}$$

where

$$\mathbf{M}(\boldsymbol{\Lambda}) := \left\{ \boldsymbol{\Delta} \in RH_\infty : \boldsymbol{\Delta}(s_0) \in \boldsymbol{\Lambda} \ \text{ for all } \ s_0 \in \overline{C}_+ \right\}$$

$$\boldsymbol{\Lambda} = \left\{ diag\left[\delta_1 \mathbf{I}_{r1}, \ldots, \delta_s \mathbf{I}_{rS}, \boldsymbol{\Delta}_1, \ldots \boldsymbol{\Delta}_F\right] : \delta_i \in C, \boldsymbol{\Delta}_j \in C^{m_j \times n_j} \right\},$$

$$\sum_i r_i + \sum_j m_j = M_1, \quad \sum_i r_i + \sum_j n_j = N_1$$

S and F represent the number of repeated scalar and full blocks, respectively. C is the

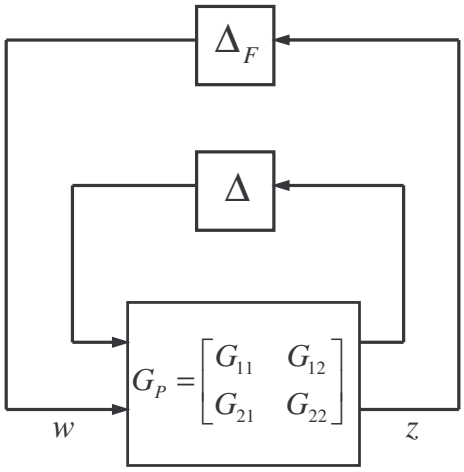

Figure 8. Loop diagram of the system for robust stability and robust performance analyses [30].

field of complex numbers and $\overline{C}_+$ *represents the closed right half plane.*

Theorem 2[30] (Robust Performance): *Let* $\beta>0$. *For all* $\boldsymbol{\Delta} \in \mathbf{M}(\boldsymbol{\Lambda})$ *with* $\|\boldsymbol{\Delta}\|_\infty < \frac{1}{\beta}$, *the loop shown in Figure 8 is well-posed and internally stable and* $\|F_u(\mathbf{G}_\mathrm{P}, \boldsymbol{\Delta})\|_\infty \le \beta$ *if and only if*

$$\sup_{\omega \in \Re} \mu_{\boldsymbol{\Lambda}_\mathrm{P}}(\mathbf{G}_\mathrm{P}(j\omega)) \le \beta \tag{17}$$

where F_u *is the upper fractional transformation operator,* $\mathbf{M}(\boldsymbol{\Lambda})$ *is the same as in Theorem 1, and*

$$\boldsymbol{\Lambda}_\mathrm{P} = \left\{ \begin{bmatrix} \boldsymbol{\Delta} & \mathbf{0} \\ \mathbf{0} & \boldsymbol{\Delta}_\mathrm{f} \end{bmatrix} : \boldsymbol{\Delta} \in \boldsymbol{\Lambda}, \boldsymbol{\Delta}_\mathrm{f} \in C^{M_2 \times N_2} \right\}$$

M_2 and N_2 are the overall dimensions of w and z in Figure 8 respectively.

4.1. Perturbation of stiffness due to nonlinearity

The principal nonlinearity in a building is due to yielding of structural elements. As the end deformation of a structural column or beam exceeds its yield limit, the incremental behavior of the element is characterized by a reduced tangent stiffness on the force-deformation relation. Depending on the number of yielded elements and the extent of yielding in each member, the total stiffness of the structure degrades from its initial state to a substantially reduced state.

An equivalent shear model of a building structure is proposed to clearly identify stiffness nonlinearities for use in perturbation analyses. Suppose the story stiffness degrades from the maximum initial stiffness k_{ini} to the minimum post-yield stiffness k_{py} following complete formation of plastic hinges in a given story. The post-yield stiffnesses can be inferred from the story force-deformation relations of a complete model of the structure. An initial stiffness matrix $\mathbf{K}_{\text{ini}}$ for the equivalent shear model, constructed from the elastic story stiffnesses, is

$$\mathbf{K}_{\text{ini}} = \begin{bmatrix} k_{\text{ini},1} + k_{\text{ini},2} & -k_{\text{ini},2} & & \\ -k_{\text{ini},2} & \ddots & \ddots & \\ & \ddots & k_{\text{ini},n-1} + k_{\text{ini},n} & -k_{\text{ini},n} \\ & & -k_{\text{ini},n} & k_{\text{ini},n} \end{bmatrix} \tag{18}$$

The mass matrix for the equivalent shear model $\mathbf{M}_{\text{SM}}$ is a diagonal lumped mass matrix, and Rayleigh damping is used to generate the damping matrix $\mathbf{C}_{\text{SM}}$.

As the building yields, the values of individual story stiffnesses vary, but the structure of the stiffness matrix in Equation (18) is preserved. To treat story stiffnesses $k_{\text{ini},i}$ as perturbed stiffness components, the matrix $\mathbf{K}_{\text{ini}}$ is transformed to a matrix $\mathbf{K}_{\text{d}}$ in terms of drift degrees of freedom:

$$\mathbf{K}_{\text{ini}} = \mathbf{T}^{\text{T}}\mathbf{K}_{\text{d}}\mathbf{T}, \quad \mathbf{T} = \begin{bmatrix} 1 & & & 0 \\ -1 & 1 & & \\ & \ddots & \ddots & \\ 0 & & -1 & 1 \end{bmatrix}_{n\times n}, \quad \mathbf{K}_{\text{d}} = diag\left(\left[k_{\text{ini},1}, \cdots, k_{\text{ini},n}\right]\right) \tag{19}$$

where $\mathbf{T}$ is the transformation matrix from displacements to drifts. The stiffness perturbations caused by structure nonlinearity are modeled by multiplicative perturbations as follows:

$$\overline{\mathbf{K}} = \left[\left(\mathbf{I} - \frac{\mathbf{A}_{\text{k}}}{2}\right) + \frac{\mathbf{A}_{\text{k}}}{2}\mathbf{\Delta}_{\text{k}}\right]\mathbf{K}_{\text{d}} \tag{20}$$

where $\mathbf{\Delta}_{\text{k}}$ and $\mathbf{A}_{\text{k}}$ are

$$\mathbf{\Delta}_{\text{k}} = diag\left(\left[\delta_{\text{k}1}, \cdots, \delta_{\text{k}n}\right]\right), \quad \left|\delta_{\text{k}i}\right| \le 1, \quad \mathbf{A}_{\text{k}} = diag\left(\left[\alpha_{\text{k}1}, \cdots, \alpha_{\text{k}n}\right]\right) \tag{21}$$

and

$$\alpha_{\text{k}i} = \left(\frac{k_{\text{ini}} - k_{\text{py}}}{k_{\text{ini}}}\right)_i \tag{22}$$

The diagonal stiffness $\overline{\mathbf{K}}$ represents a perturbation of the story stiffness about reference stiffness $(k_{\text{ini},i}+k_{\text{py},i})/2$ that is midway between the initial elastic and post-yield stiffness of each story. For $\overline{\mathbf{K}}$ defined as in Equation (20) and for all possible $\mathbf{\Delta}_{\text{k}}$ (Equation (21)), $\left\|\overline{\mathbf{K}}\right\|_\infty \le \left\|\mathbf{K}_{\text{d}}\right\|_\infty$.

The loop diagram of the system with specified perturbations is shown in Figure 9, where $\mathbf{K}_{\text{co}}$ represents the controller and $\mathbf{W}_{\text{drift}}$, $\mathbf{W}_{\text{acc}}$, and $\mathbf{W}_{\text{uco}}$ represent weighting filters on the story drift, absolute acceleration, and control force respectively. The standard

diagram for perturbation analysis is shown in Figure 10. Based on the system loop diagram (Figure 9), input-output relations for the standard model (Figure 10) are as follows:

$$\begin{bmatrix} \mathbf{y}_{\mathrm{k}} \\ \mathbf{y}_{\mathrm{out}} \\ \mathbf{y}_{\mathrm{co}} \end{bmatrix} = \mathbf{P}\mathbf{u}_{\mathrm{p}},\ \mathbf{P} = \begin{bmatrix} \mathbf{P}_{\Delta} \\ \mathbf{P}_{\mathrm{in-out}} \\ \mathbf{P}_{\mathrm{co}} \end{bmatrix},\ \mathbf{u}_{\mathrm{p}} = \begin{bmatrix} \mathbf{u}_{\mathrm{k}} \\ \ddot{\mathbf{x}}_{\mathrm{g}} \\ \mathbf{v} \\ \mathbf{u}_{\mathrm{co}} \end{bmatrix},\ \mathbf{y}_{\mathrm{out}} = \begin{Bmatrix} \mathbf{x}_{\mathrm{drift}} \\ \ddot{\mathbf{x}}_{\mathrm{abs}} \\ \mathbf{u}_{\mathrm{co}} \end{Bmatrix} \tag{23}$$

where $\mathbf{P}_{\Delta}$ is the transfer matrix relating the input $\mathbf{u}_{\mathrm{p}}$ to the stiffness perturbation matrix $\mathbf{y}_{\mathrm{k}}$. Similarly, $\mathbf{P}_{\text{in-out}}$ and $\mathbf{P}_{\mathrm{co}}$ represent transfer matrices from input $\mathbf{u}_{\mathrm{p}}$ to regulated outputs $\mathbf{y}_{\mathrm{out}}$ and controller inputs $\mathbf{y}_{\mathrm{co}}$ respectively. The state space representation of the plant

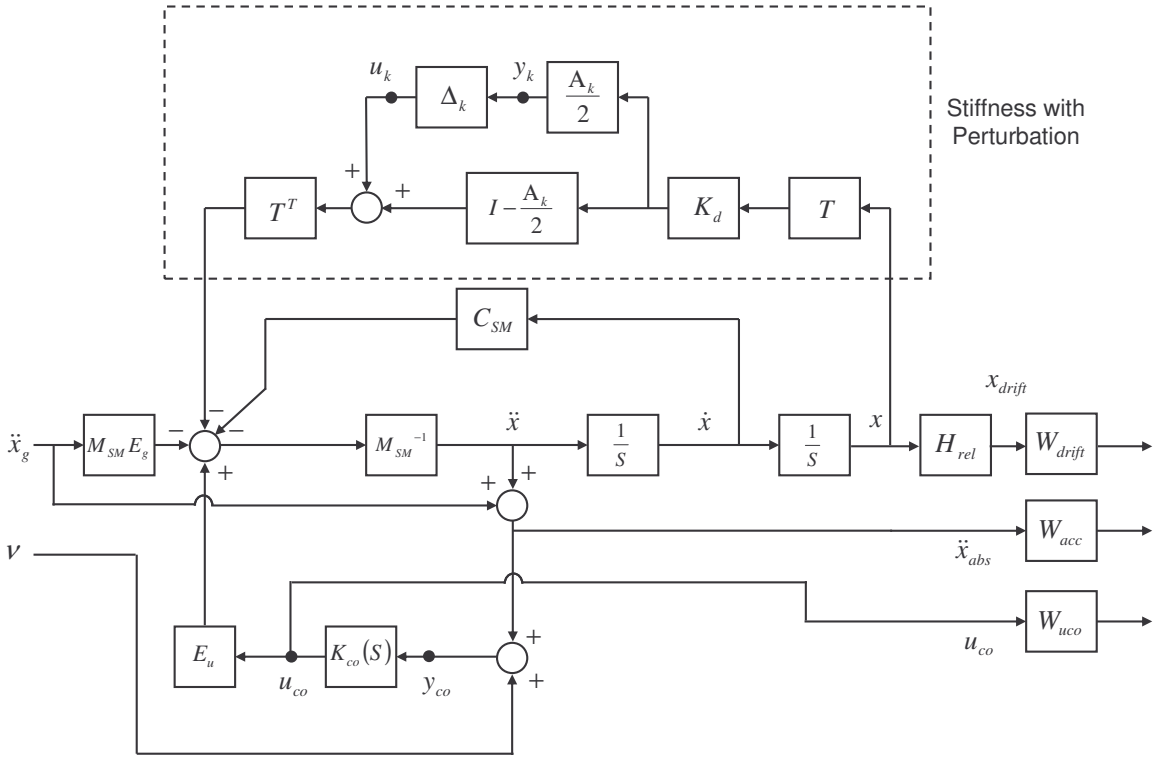

Figure 9. Loop diagram of the system with stiffness perturbation.

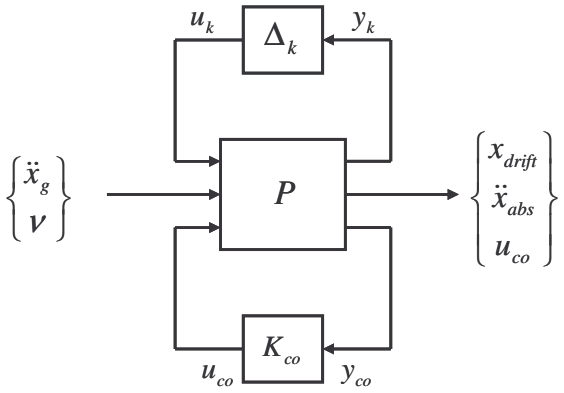

Figure 10. Standard diagram for perturbation analysis.

model **P** in Figure 6, which deviates from the representation of the original model in Equation (2a), is determined based on the loop diagram of the system in Figure 9, and represented by the following equations:

$$\dot{\mathbf{z}}_{\mathrm{p}} = \mathbf{A}_{\mathrm{p}}\mathbf{z}_{\mathrm{p}} + \mathbf{B}_{\mathrm{p}}\mathbf{u}_{\mathrm{p}} \tag{24}$$

where

$$\mathbf{z}_{\mathrm{p}} = \begin{Bmatrix} \mathbf{x} \\ \dot{\mathbf{x}} \end{Bmatrix},\ \mathbf{A}_{\mathrm{p}} = \begin{bmatrix} \mathbf{0} & \mathbf{I} \\ -\mathbf{M}_{\mathrm{SM}}{}^{-1}\mathbf{T}^{\mathrm{T}}\left(\mathbf{I} - \dfrac{\mathbf{A}_{\mathrm{k}}}{2}\right)\mathbf{K}_{\mathrm{d}}\mathbf{T} & -\mathbf{M}_{\mathrm{SM}}{}^{-1}\mathbf{C}_{\mathrm{SM}} \end{bmatrix} \tag{25a}$$

$$\mathbf{B}_{\mathrm{p}} = \begin{bmatrix} \mathbf{0} & \mathbf{0} & \mathbf{0} & \mathbf{0} \\ -\mathbf{M}_{\mathrm{SM}}{}^{-1}\mathbf{T}^{\mathrm{T}} & -\mathbf{E}_{\mathrm{g}} & \mathbf{0} & \mathbf{M}_{\mathrm{SM}}{}^{-1}\mathbf{E}_{\mathrm{u}} \end{bmatrix} \tag{25b}$$

Taking the Laplace transform of Equation (24), $\mathbf{Z}_{\mathrm{p}}$ is found to be

$$\mathbf{Z}_{\mathrm{p}} = \left(s\mathbf{I} - \mathbf{A}_{\mathrm{p}}\right)^{-1}\mathbf{B}_{\mathrm{p}}\mathbf{U}_{\mathrm{p}} \tag{26}$$

Based on previously defined parameters and Equation (26), $\mathbf{P}_{\Delta}$ is

$$\mathbf{P}_{\Delta} = \frac{\mathbf{A}_{\mathrm{k}}}{2}\mathbf{K}_{\mathrm{d}}\mathbf{T}\begin{bmatrix}\mathbf{I} & \mathbf{0}\end{bmatrix}\left(s\mathbf{I} - \mathbf{A}_{\mathrm{p}}\right)^{-1}\mathbf{B}_{\mathrm{p}} \tag{27}$$

Similarly, $\mathbf{P}_{\text{in-out}}$ is defined as

$$\mathbf{P}_{\mathrm{in-out}} = \mathbf{C}_{\mathrm{in-out}}\left(s\mathbf{I} - \mathbf{A}_{\mathrm{p}}\right)^{-1}\mathbf{B}_{\mathrm{p}} + \mathbf{D}_{\mathrm{in-out}} \tag{28a}$$

$$\mathbf{C}_{\mathrm{in-out}} = \begin{bmatrix} \mathbf{H}_{\mathrm{rel}} & \mathbf{0} \\ -\mathbf{M}_{\mathrm{SM}}{}^{-1}\mathbf{T}^{\mathrm{T}}\left(\mathbf{I} - \frac{\mathbf{A}_{\mathrm{k}}}{2}\right)\mathbf{K}_{\mathrm{d}}\mathbf{T} & -\mathbf{M}_{\mathrm{SM}}{}^{-1}\mathbf{C}_{\mathrm{SM}} \\ \mathbf{0} & \mathbf{0} \end{bmatrix} \tag{28b}$$

$$\mathbf{D}_{\mathrm{in-out}} = \begin{bmatrix} \mathbf{0} & \mathbf{0} & \mathbf{0} & \mathbf{0} \\ -\mathbf{M}_{\mathrm{SM}}{}^{-1}\mathbf{T}^{\mathrm{T}} & \mathbf{0} & \mathbf{0} & \mathbf{M}_{\mathrm{SM}}{}^{-1}\mathbf{E}_{\mathrm{u}} \\ \mathbf{0} & \mathbf{0} & \mathbf{0} & \mathbf{I} \end{bmatrix} \tag{28c}$$

and $\mathbf{P}_{\mathrm{co}}$ is found to be

$$\mathbf{P}_{\mathrm{co}} = \mathbf{C}_{\mathrm{co}}\left(s\mathbf{I} - \mathbf{A}\right)^{-1}\mathbf{B}_{\mathrm{p}} + \mathbf{D}_{\mathrm{co}} \tag{29a}$$

$$\mathbf{C}_{\mathrm{co}} = \begin{bmatrix} -\mathbf{M}_{\mathrm{SM}}{}^{-1}\mathbf{T}^{\mathrm{T}}\left(\mathbf{I} - \frac{\mathbf{A}_{\mathrm{k}}}{2}\right)\mathbf{K}_{\mathrm{d}}\mathbf{T} & -\mathbf{M}_{\mathrm{SM}}{}^{-1}\mathbf{C}_{\mathrm{SM}} \end{bmatrix} \tag{29b}$$

$$\mathbf{D}_{\mathrm{co}} = \begin{bmatrix} -\mathbf{M}_{\mathrm{SM}}{}^{-1}\mathbf{T}^{\mathrm{T}} & \mathbf{0} & \mathbf{I} & \mathbf{M}_{\mathrm{SM}}{}^{-1}\mathbf{E}_{\mathrm{u}} \end{bmatrix} \tag{29c}$$

Using the lower fractional transformation operator F_l, the combined structure-controller model $\mathbf{G}_{\mathrm{P}}$ in Theorems (1) and (2) is

$$\mathbf{G}_{\mathrm{P}} = F_l\left(\mathbf{P}, \mathbf{K}_{\mathrm{co}}\right) \tag{30}$$

5. APPLICATION TO AN EXAMPLE STRUCTURE

5.1. System considered (benchmark structure)

The system considered in this study is a 3-story steel building designed by Brandow & Johnston Associates for the SAC steel project that has been widely used as a benchmark to evaluate the efficiency of control methods [32-34]. The building was designed to meet the seismic code requirements of the 1994 UBC for a location in Los Angeles, California. The lateral seismic loads are resisted by perimeter moment resisting frames (MRF) in each direction, and the model is simplified to a single multi-bay MRF that carries half of the seismic mass of the floor at each story level in the horizontal direction and 1/6 of the story gravity load in the vertical direction. The elevation view of the model frame is shown in Figure 11 with moment connections indicated by dots. A finite element model of the frame in Matlab has been provided by [34] for benchmark control evaluation, and is utilized here. In the model, the columns are assumed to remain elastic, while the moment-rotation response of the beams is elastic-perfectly plastic with a nonlinear transition from the initial to post-yield region. Rayleigh damping is applied to the frame, calibrated to a damping ratio ξ=4.3% in the first and third modes. Consistent with the benchmark problem definition, the damping matrix is proportional to the initial elastic stiffness of the structure regardless of the observed nonlinear response, even though this assumption can overestimate the effects of viscous energy dissipation [35]. The first three natural frequencies of the structure are: 0.99, 3.06, and 5.83 Hz. The control devices consist of ideal actuators applied at each level, whose force capacities are to be determined based on performance objectives.

Three bins of motions developed for the SAC project are selected here to evaluate

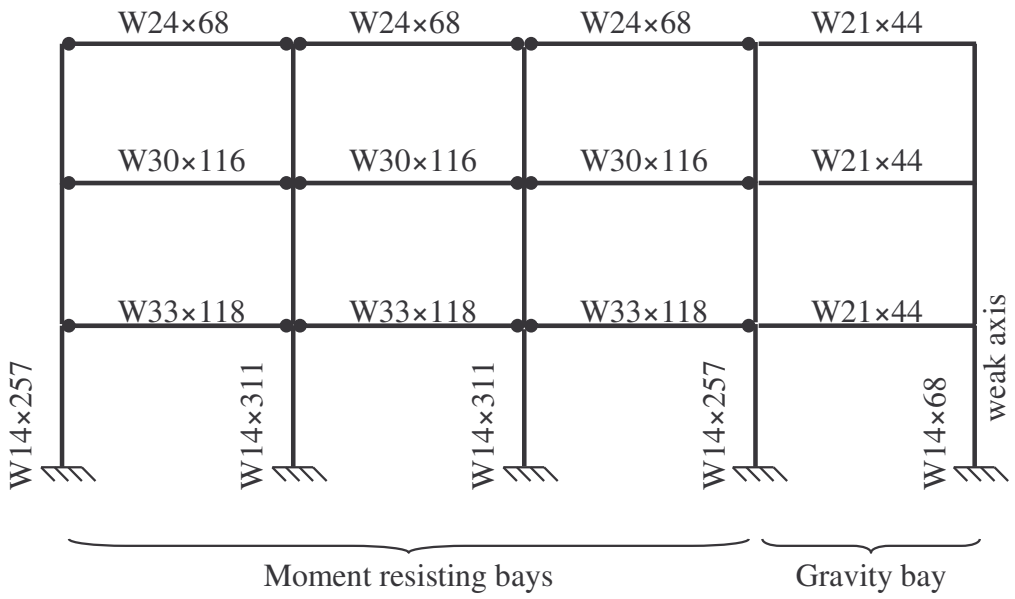

Figure 11. Elevation view of the lateral moment frame for the 3-story benchmark building [34]. Moment connections are indicated by dots.

the controller performance using nonlinear response history analysis. The three bins – containing 60 total motions – represent a 2%, 10%, and 50% probability of exceedance (PE) in 50 years for a Los Angeles, California site with soil type S_D.

5.2. H_2/ LQG controller

An H_2/LQG controller is designed based on a reduced order model provided in the benchmark problem [34]. In the reduced order model, frame members are assumed to be axially rigid, and rotational degrees of freedom are eliminated by static condensation, leaving only 3 lateral degrees of freedom. The natural frequencies of the reduced order model are 0.98, 2.98, and 5.69 Hz, which are close to the first three natural frequencies of the complete model.

The following performance objectives are selected for the controlled system: maximum story drift ≤ 2%, maximum story acceleration ≤ 1.4 g, and maximum number

of plastic hinges ≤ 6 for any ground excitation in the three bins. The performance objectives selected by designers should reflect careful consideration of the tradeoff in cost versus performance. The objective of linear (damage free) structural response is appropriate if it can be reasonably attained. For this example, linear response was achievable but with very large control forces (4400 kip for a single story). The selected performance objectives balance cost and performance while achieving an important objective of this study, to improve controller performance in nonlinear structures.

From numerical results, the minimum story control force that satisfies the performance objective is found to be around 2700 kips, which is assumed to be achievable. For this control force, numerical simulations were performed to search among several combinations of gain matrix parameters to minimize the story drifts and floor accelerations. The resulting design parameters are: α_1=5e-8, α_2=1e-6, p=0.5. This controller is intended to represent the best H_2/LQG control design without pre-filters.

5.3. Pre-filters to controller

Two pre-filters $f_{\text{pre drift}}$ and $f_{\text{pre acc}}$ (Figure 12(a)) have been selected to minimize the maximum SV of drift and total acceleration transfer matrices, respectively, in the 0.5 to 15 Hz frequency range, without restricting the maximum control force. Adding the pre-filter $f_{\text{pre drift}}$ (l=8 Hz, a=0.825, b=1, and c=0.95) reduces the maximum SV of the drift transfer matrix from 4 Hz to 11 Hz and the total acceleration transfer matrix from 1 Hz to 9 Hz (Figures 12(b) and (c)) relative to the reference H_2/LQG controller. Since $f_{\text{pre drift}}$ considerably increases the maximum SV of the absolute acceleration and control force transfer matrices at frequencies larger than 9 Hz (Figures 12(c) and (d)), absolute acceleration and control force demands are expected to increase in the time domain.

Adding the pre-filter $f_{pre\ acc}$ (l=26 Hz, a=0.775, b=1.05, and c=1) maintains or reduces the maximum SV of the total acceleration transfer matrix for frequencies less than 30 Hz (Figure 12(c)) and slightly reduces the maximum SV of the drift transfer matrix for frequencies above 8 Hz (Figure 12(b)) relative to the reference H_2/LQG controller. The increase in absolute acceleration SV for frequencies above 30 Hz is of concern only if the earthquake contains significant energy in the high frequency range. Adding $f_{pre\ acc}$ leads to a reduction in the maximum SV of the control force transfer matrix for frequencies below 12 Hz but a substantial increase beyond 12 Hz, suggesting that the control force demands will be larger for most of the earthquakes (Figure 12(d)).

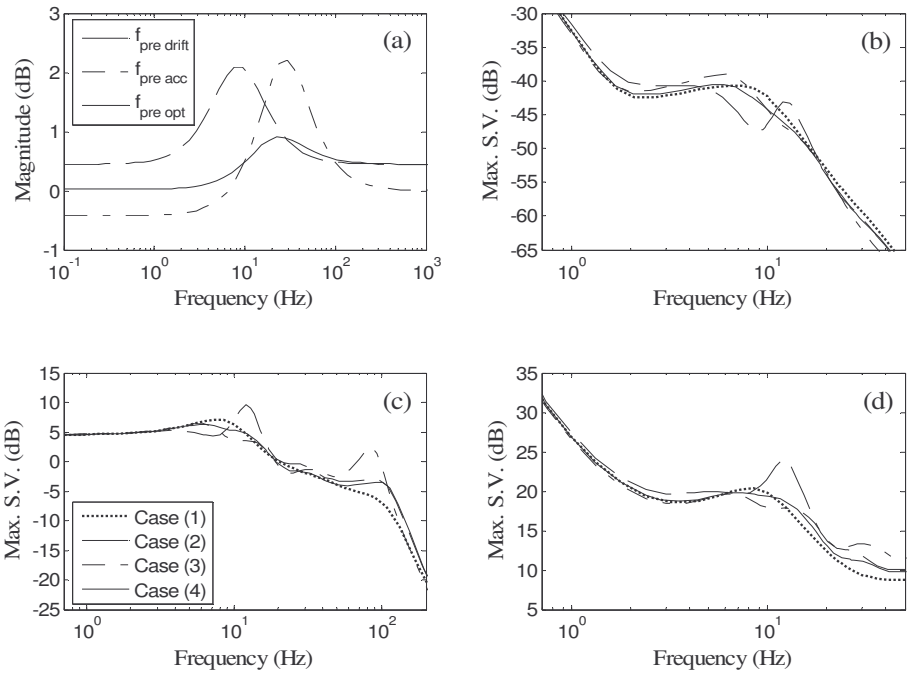

Figure 12. Frequency response of input-output transfer matrices for reference controller with various pre-filters, including: (a) the shape of the filters, (b) maximum SV of the transfer matrix from input to story drifts, (c) maximum SV of the transfer matrix from input to absolute acceleration, and (d) maximum SV of the transfer matrix from input to control force.

variables in the filter, where the search range is narrowed by first assessing the controller performance in the frequency domain. Consequently, the search range includes only pre-filter parameters that reduce the average maximum SV of the transfer matrices for both drift and absolute acceleration from 0.5 Hz to 15 Hz relative to the H_2/LQG controller. Figure 13 indicates the response reduction in the maximum story drift, absolute acceleration, and control force in the time domain with respect to varied filter parameters a and l (b=0.95 and c=1).

The parameters of the optimal filter $f_{pre\ opt}$ – shown by the black circles in Figure 9 – are l=20 Hz, a= 0.95, b=1.05, and c=0.95. Maximum SV frequency responses of the system with $f_{pre\ opt}$ (Figures 12(b)-(d)), which are reduced over a wide frequency range relative to H_2/LQG, suggest that the controller will be effective in reducing response in the time domain.

The results of nonlinear time history analyses of the building with different controllers subjected to the 3 ground acceleration bins described previously are presented in Table 4. As expected, pre-filters $f_{pre\ drift}$ and $f_{pre\ acc}$ improve drift and acceleration responses, respectively, with respect to the H_2/LQG controller, but degrade the response in other measures. The optimal pre-filter, on the other hand, is seen to reduce the values of nearly all response measures. For the largest 2% PE in 50 (2 in 50) year acceleration bin, peak and residual drifts are reduced by 9.3% and 18.4% compared to H_2/LQG. The peak and RMS accelerations decrease by 0.3% and 2.5% respectively, and the maximum control force increases by a minor 1.0%. Compared to H_2/LQG, the number of plastic hinges drops for the 10 in 50 and 50 in 50 year bins and is unaffected for the 2 in 50 year bin. In summary, the optimal pre-filter consistently reduces both drift and acceleration to

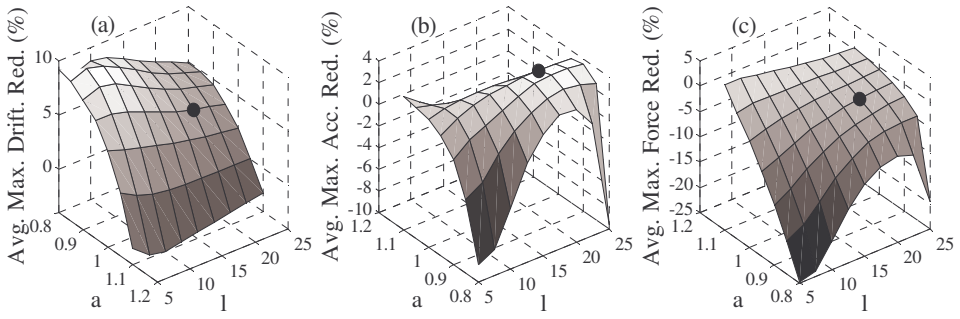

Figure 13. Reductions in (a) average drift, (b) average absolute acceleration, and (c) average required control force of the system enhanced with pre-filter relative to H_2/LQG as a function of filter parameters *a* and *l* (b=0.95 and c=1).

achieve superior performance. As a side note, each controller reduces the structural response substantially compared to the uncontrolled system and the effectiveness of the pre-filters should be considered in this context [Table 4].

5.4. Demonstration of robust stability and performance

Applying the combined structure/controller model of Equation (30) and Figure 9, Theorems (1) and (2) are applied to investigate robustness of stability and performance of the example structure with different controllers subjected to uncertainties in the stiffness matrix. The story force-deformation relation for each story level is characterized through a nonlinear static analysis of the unreduced structure model subjected to linear lateral load distribution over the height of the structure (Figure 14). Initial stiffnesses k_{ini} and post-yield story stiffnesses k_{py} derived from the story force-deformation relations are reported in Table 5. The first three natural frequencies of the equivalent shear model based on initial stiffness are 0.99 Hz, 2.52 Hz, and 3.84 Hz, where the first natural frequency matches that of the unreduced model.

To verify stability robustness, structured singular values of the first block in the

system transfer matrix $\mu_{\Delta}(\mathbf{G}_{11}(j\omega))$ are found through μ analysis (Theorem 1). Both the H_2/LQG controller and the controller with optimal pre-filter are robustly stable considering the maximum stiffness variation in either direction (Figure 15(a)). As the entries of matrix $\mathbf{A}_k$ (Equation (21)) represent the maximum magnitude of stiffness deviation from the nominal state, the parameter β=1 (Equation (16)). Therefore, to be robustly stable, μ is required everywhere to be ≤1, which is true for both controllers (Figure 15(a)). The upper bound maximum SV μ=0.84 indicates that the system remains stable for diagonal perturbations smaller than 1/0.84. Including a pre-filter has negligible influence on the μ values, and therefore does not affect the overall stability robustness (Figure 15(a)).

To verify robustness of performance, structured singular values of the complete system transfer matrix $\mu_{\Delta}(\mathbf{G}_{P}(j\omega))$ are found through μ analysis considering the two uncertainty matrices in Figure 10 (Theorem 2). To apply Theorem 2, the bounds on the

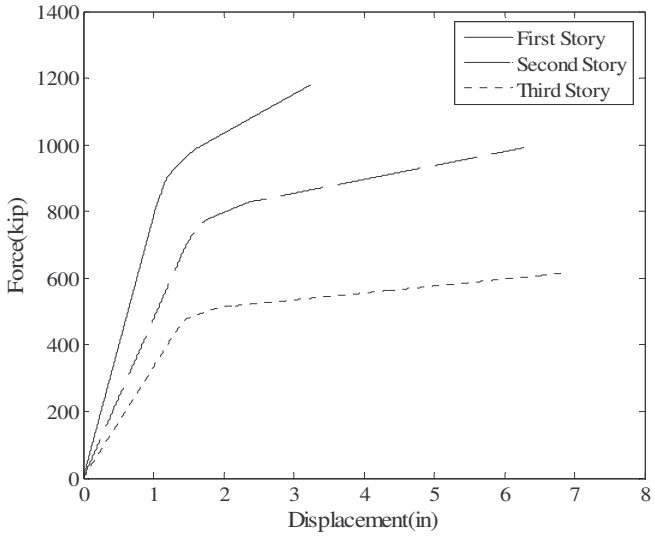

Figure 14. Story force-deformation relations for the unreduced structure model

Table 4. Response of the structure for the uncontrolled case together with the response of the structure with H_2/LQG controller without pre-filter, with $f_{pre\ drift}$, $f_{pre\ acc,}$ and $f_{pre\ opt}$ subjected to 60 SAC LA ground motions.

Controller Type	Probability of Exceedance in 50 Years	Mean						Max					
		Max. Drift (%)	Res. Drift (%)	Max. Acc. (g)	RMS Acc. (g)	No. P. H.	Max. Force(kip)	Max. Drift (%)	Res. Drift (%)	Max. Acc. (g)	RMS Acc. (g)	No. P. H.	Max. Force(kip)
Uncontrolled	10%	2.56	0.694	0.81	0.15	17.40		4.82	1.759	1.54	0.21	18.00	
	2%	5.76	1.168	1.11	0.19	18.00		12.06	4.395	1.95	0.24	18.00	
	50%	1.43	0.172	0.66	0.13	10.60		4.57	0.771	1.28	0.17	18.00	
H_2/LQG without pre-filter	10%	0.55	0.018	0.54	0.08	0.20	1118	0.83	0.123	0.80	0.12	2.00	1699.40
	2%	0.97	0.072	0.88	0.14	3.00	1852.3	1.73	0.239	1.34	0.19	6.00	2670.20
	50%	0.30	0.016	0.35	0.05	0.30	663.51	1.06	0.091	0.91	0.12	6.00	1735.10
H_2/LQG with $f_{pre\ drift}$	10%	0.51	0.023	0.58	0.09	0.00	1737.30	0.81	0.108	1.13	0.13	0.00	2124.90
	2%	0.84	0.035	0.94	0.15	2.50	2775.00	1.27	0.189	1.81	0.21	6.00	3372.70
	50%	0.26	0.015	0.38	0.06	0.00	1634.30	0.67	0.049	0.84	0.12	0.00	1952.80
H_2/LQG with $f_{pre\ acc}$	10%	0.53	0.020	0.51	0.08	0.10	1192.00	0.83	0.123	0.73	0.11	2.00	1808.10
	2%	0.97	0.074	0.86	0.13	3.70	1878.60	1.69	0.256	1.31	0.17	12.00	2604.90
	50%	0.30	0.014	0.38	0.05	0.10	828.88	0.93	0.077	0.89	0.10	2.00	1774.50
H_2/LQG with $f_{pre\ opt}$	10%	0.53	0.018	0.51	0.08	0.00	1157.00	0.81	0.071	0.80	0.12	0.00	1739.00
	2%	0.92	0.056	0.85	0.14	3.00	1880.60	1.57	0.195	1.34	0.19	6.00	2697.60
	50%	0.29	0.012	0.34	0.05	0.10	705.82	0.95	0.049	0.83	0.11	2.00	1704.70

Table 5. Initial and post-yield stiffnesses of each story.

	Stiffness (kip/in)	
	Initial	post-yield
Story No	(k_{ini})	(k_{py})
1	782.8	117.4
2	477.7	41.7
3	333.5	20.9

system outputs are introduced through weighting filters $\mathbf{W}_{drift}$, $\mathbf{W}_{acc}$, and $\mathbf{W}_{uco}$ (Figure 9). These weighting matrices normalize the response by the target values corresponding to the performance objectives selected for controller design (story drift ≤ 2%, story acceleration ≤ 1.4 g, and control force ≤ 2700 kips). Therefore, weighting matrices have the following form:

$$\mathbf{W}_{drift} = \frac{1}{0.02h} diag([1 \quad 1 \quad 1]) \tag{31a}$$

$$\mathbf{W}_{acc} = \frac{1}{1.4g} diag([1 \quad 1 \quad 1]) \tag{31b}$$

$$\mathbf{W}_{uco} = \frac{1}{2700} diag([1 \quad 1 \quad 1]) \tag{31c}$$

where h is the height of one story (h=156 in).

Structured singular values of the perturbed system for the H_2/LQG and optimal pre-filter controllers are presented in Figure 15(b). The peaks of the structured singular values are slightly larger than 1 for both controllers at very low frequencies (Figure 11(b)). Therefore, nonlinearly responding systems with optimal

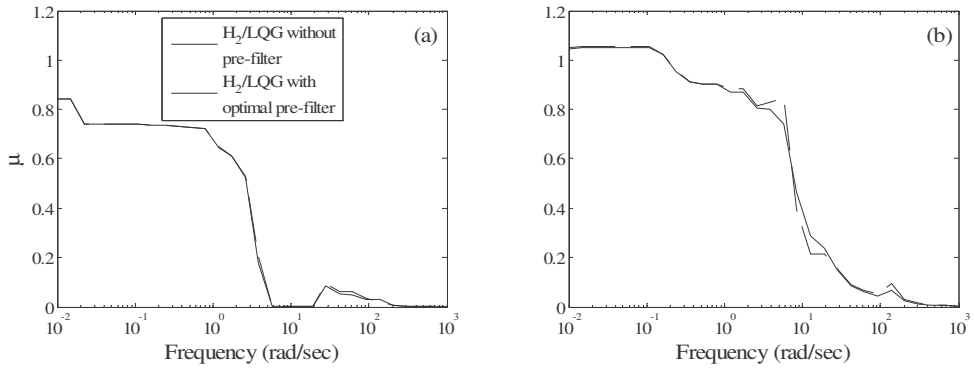

Figure 15. Structured singular values for (a) robust stability and (b) robust performance analysis.

controllers are nearly robust in performance. While the relative μ values of the optimal pre-filter controller show frequency dependent variation with respect to the H_2/LQG controller, the variations are rather insignificant and do not affect the upper bound μ, and performance robustness can also be concluded to be unaffected by pre-filters.

6. CONCLUSIONS

The effectiveness of applying a frequency dependent pre-filter to an H_2/LQG controller to improve the controlled response of a nonlinear structure was investigated in this study. These pre-filters provide control on the shape of the maximum SV response of input-output transfer matrices, which is used to minimize response measures over frequencies of concern. Optimal H_2/LQG controllers with and without pre-filters were designed for an example SAC nonlinear 3-story steel building, and the performance of the structure with different pre-filters was evaluated by nonlinear response history analysis using 60 SAC ground motions. The following conclusions are drawn regarding the use of pre-filters:

- Maximum SV response of transfer matrices is a good predictor of the resultant performance in the time domain, even when the controlled structure is lightly nonlinear.
- Specific response measures such as drift and total acceleration can be further reduced in the time domain through the application of pre-filters that reduce the corresponding response over a target frequency range.
- An optimal pre-filter can be found that consistently reduces essentially all response measures compared to the controller without pre-filter, without increase in the maximum control force.
- Application of pre-filters leads to considerable reduction in the maximum peak response over all 60 SAC motions, but the reduction in mean peak response is not significant.

Furthermore, a generally applicable framework to evaluate robustness of the stability and performance of nonlinear responding structures was developed. In the proposed perturbation model, uncertainties are treated as perturbations of individual stiffness components, and the more accurate structured singular value analysis (μ analysis) can be applied. Since the variations in stiffness are bounded by the initial and the post-yield stiffness, the nominal model for robustness evaluation represents a structure with stiffness matrix midway between the maximum (initial linear) and minimum (fully yielded) states. Consequently, uncertainties are symmetric with respect to the nominal model. Structured singular values derived by μ analysis for the SAC structure demonstrated that the optimal H_2/LQG controller with and without pre-filter is completely robust in stability and nearly robust in performance with

respect to the performance objectives considered for the structure.

REFERENCES

1. Spencer Jr BF, Nagarajaiah S. State of the art of structural control. *Journal of Structural Engineering* 2003; **129**(7):845–56.

2. Dyke SJ. Current directions in structural control in the US. *Proceedings of the 9th World Seminar in Seismic Isolation, Energy Dissipation and Active Vibration Control of Structures*, Kobe, Japan, June 2005.

3. Safonov MG, Athans M. Gain and phase margins for multiloop LQG regulators. *IEEE Transaction on Automatic Control* 1977; **22**:173–179.

4. Soong TT. *Active Structural Control: Theory and Practice*, Longman Scientific and Technical, Essex: England, 1990.

5. Dyke SJ, Yi F. On the performance of controlled civil engineering structures. *Proceedings of Structures Congress 2000*, Philadelphia, Pennsylvania, May 2000.

6. Wu JC, Yang JN. LQG control of lateral-torsional motion of Nanjing TV transmission tower. *Earthquake Engineering and Structural Dynamics* 2000; **29**(8):1111–1130.

7. Christenson RE, Spencer Jr BF, Johnson EA. Semiactive connected control method for adjacent multidegree-of-freedom buildings. *Journal of Engineering Mechanics* 2007; **133**(3):290–298.

8. Park KS, Koh HM, Ok SY, Seo CW. Fuzzy supervisory control of earthquake-excited cable-stayed bridges. *Engineering Structures* 2005; **27**(7):1086–1100.

9. Chang-Hee W, Sain MK, Spencer Jr BF. Performance and stability characteristics of risk sensitive controlled structures under seismic disturbances. *Proceedings of American Control Conference*, Seattle, Washington, June 1995.

10. Wang SG. Linear quadratic Gaussian-alpha control with relative stability and gain parameter for the structural benchmark problems. *Journal of Engineering Mechanics* 2004; **130**(4):511–517.

11. Adhikari R, Yamaguchi H, Yamazaki T. Modal space sliding-mode control of structures. *Earthquake Engineering and Structural Dynamics* 1998; **27**(11):1303–1314.

12. Shafieezadeh A, Ryan KL, Chen YQ. Fractional order filter enhanced LQR for seismic protection of civil structures. *Journal of Computational and Nonlinear Dynamics* 2008; **3**

13. Chase JG, Barroso LR, Hunt S. Quadratic jerk regulation and the seismic control of civil structures. *Earthquake Engineering and Structural Dynamics 2003;* **32**(13):2047–2062.

14. Ankireddi S, Yang HTY. Multiple objective LQG control of wind-excited buildings. *Journal of Structural Engineering* 1997; **123**(7):943–951.

15. Adeli H, Kim H. Wavelet-hybrid feedback least mean square algorithm for robust control of structures. *Journal of Structural Engineering* 2004; **130**(1):128–137.

16. Soong TT, Grigoriu M. *Random Vibration of Mechanical and Structural Systems.* Prentice Hall: Englewood Cliffs, New Jersey, 1993.

17. Suhardjo J, Spencer Jr BF, Kareem A. Frequency domain optimal control of wind-excited buildings 1992. *Journal of Engineering Mechanics* 1992; **118**(12):2463–2481.

18. Spencer Jr BF, Suhardjo J, Sain MK. Frequency domain optimal control strategies for aseismic protection. *Journal of Engineering Mechanics* 1994; **120**(1):135–159.

19. Min KW, Chung L, Joo SJ, Kim J. Design of frequency dependent weighting functions for H_2 control of seismic excited structures. *Journal of Vibration and Control* 2005; **11**(1): 137–157.

20. Doyle JC. Guaranteed margins for LQG regulators. *IEEE Transaction on Automatic Control* 1978; **AC-23**(4):756–757.

21. Diersing RW, Sain MK. A multiobjective cost cumulant control problem: the Nash game solution. *Proceedings of American Control Conference*, Portland, Oregon, June 2005.

22. Young PM, Bienkiewicz B. Robust controller design for the Active Mass Driver benchmark problem. *Earthquake Engineering and Structural Dynamics* 1998; **27**(11):1149–1164.

23. Wang SG, Roschke PN, Yeh HY. Robust control for structural systems with uncertainties. *Proceedings of the 6th Annual SPIE's International Symposium on Smart Structures and Materials, Conference on Smart Systems for Bridges, Structures, and Highways*, Long Beach, California, May, 1999.

24. Wang SG, Robust active control for uncertain structural systems with acceleration sensors, *Journal of Structural Control* 2003; **10**(1):59–76.

25. Forrai A, Hashimoto S, Isojima A, Funato H, Kamiyama K. Gray box identification of flexible structures: application to robust active vibration suppression control. *Earthquake Engineering and Structural Dynamics* 2001; **30**(8):1203–1220.

26. Wang SG, Yeh HY, Roschke PN. Robust control for structural systems with parametric and unstructured uncertainties. *Journal of Vibration and Control* 2001; **7**(5):753–772.

27. Stavroulakisa GE, Marinovac DG, Hadjigeorgioud E, Foutsitzid G, Baniotopoulose CC. Robust Active Control Against Wind-Induced Structural Vibrations. *Journal of Wind Engineering and Industrial Aerodynamics* 2006; **94**(11):895–907.

28. Clough RW, Penzien J. *Dynamics of Structures*. McGraw-Hill: New York, 1993.

29. Chen J. Sensitivity integral relations and design trade-offs in linear multivariable feedback systems. *IEEE Transaction on Automatic Control* 1995; **40**(10):1700-1716.

30. Zhou K, Doyle JC. *Essentials of Robust Control*. Prentice Hall: Englewood Cliffs,

New Jersey, 1998.

31. Safonov MG. *Stability and Robustness of Multivariable Feedback Systems*. MIT Press: Cambridge, Massachusetts, 1980.

32. Krawinkler H, Gupta A. Story drift demands for steel moment frame structures in different seismic regions. *Proceedings of 6th National Conference on Earthquake Engineering*, Seattle, WA, 1998.

33. Gupta A. *Seismic demands for performance evaluation of steel moment resisting frame structures*, PhD thesis, Stanford University, 1999.

34. Ohtori Y, Christenson RE, Spencer Jr BF, Dyke SJ. Benchmark control problems for seismically excited nonlinear buildings. *Journal of Engineering Mechanics* 2004; **130**(4):366–385.

35. Hall JF, Problems encountered from the use (or misuse) of Rayleigh damping. *Earthquake Engineering and Structural Dynamics* 2006; **35**(5):525–545.

CHAPTER IV

CONCLUSIONS

In the first part of the study, fractional order filters are introduced in conjunction with an LQR controller. Several combinations of FOC and LQR were considered and the optimal parameters were found through numerical optimization for 64 artificially generated earthquakes. Based on simulation results, introducing the fractional order filter into the LQR controller led to a great advance in attenuating the response over optimized LQR alone. The results also showed that considering distinct fractional orders for each state variable did not appreciably improve the performance, and in some cases induced a higher structural response. Simulation results showed that the system with actual recorded ground motions give the same trend in terms of response attenuation, implying that the optimization process works well. The structure model which has been used in the study is fully observable, while this assumption is not realistic. Also, nonlinearity of the structure, time delay, and dynamics of actuators are among the issues that have not yet been investigated and should be addressed in future research.

Furthermore, the application of pre-filters to H_2/LQG controllers was investigated in this study. Singular value analysis showed that response mitigation is achievable through changing the shape of the maximum SV response of input-output transfer matrices. These reductions can be achieved in one or more response measures.

Moreover, a general perturbation model for capturing nonlinearities in robustness evaluation of structures was developed. The proposed perturbation model give the least conservative results since uncertainties are treated as perturbations of

individual stiffness components. μ analysis results for the SAC structure demonstrated that the optimal H_2/LQG controller with and without pre-filter is completely robust in stability and nearly robust in performance with respect to the performance objectives considered for the structure. Since the damping of a structure usually depends on the stiffness, nonlinear force deformation behavior of structural elements will affect the damping matrix of the whole structure. Therefore including perturbation of the damping matrix due to stiffness variations can result in more precise bounds on the smallest destabilizing perturbation bounds which is the subject of future studies.